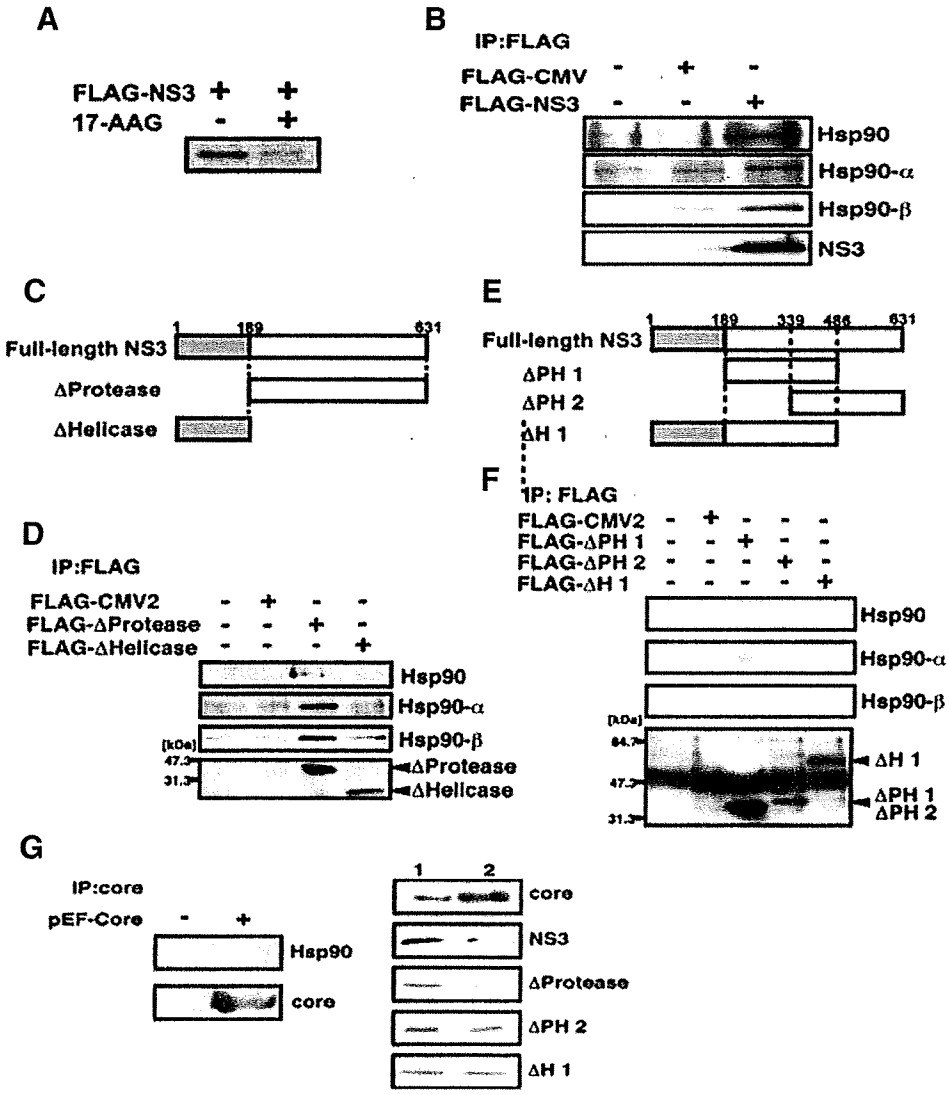

FIGURE 5. **Hsp90 regulates HCV NS3 protein stability.** *A*, Western blot showing the inhibition of NS3 protein expression in 293T cells caused by 17-AAG. Cells were transfected with pFLAG-NS3 in the presence of 250 nM 17-AAG for 48 h. *B*, FLAG-NS3 was expressed in 293T cells and immunoprecipitated (*IP*) from cell lysates with anti-FLAG antibody. Proteins immunoprecipitated were analyzed by Western blotting using anti-Hsp90, anti-Hsp90α, anti-Hsp90β, and anti-FLAG antibodies. The data shown in each *panel* are representative of three independent experiments. *FLAG-CMV*, empty plasmid vector. *C*, schematic representations of HCV NS3 protein and its deletion mutants. *D*, FLAG-NS3, FLAG-Δprotease, and FLAG-Δhelicase were expressed in 293T cells and immunoprecipitated from cell lysates with anti-FLAG antibody. Proteins immunoprecipitated with anti-Hsp90, Hsp90α, Hsp90β, and FLAG antibodies were analyzed by Western blotting. The data shown in each panel are representative of three independent experiments. *E*, schematic representations of HCV NS3 protein and further deletion mutants. *F*, FLAG-ΔPH 1, FLAG-ΔPH 2, and FLAG-ΔH 1 were expressed in 293T cells and immunoprecipitated from cell lysates with anti-FLAG antibody. Proteins immunoprecipitated with anti-Hsp90, Hsp90α, Hsp90β, and FLAG antibodies were analyzed by Western blotting. The data shown in each panel are representative of three independent experiments. *G*, FLAG-NS3, pEF-Core, FLAG-Δprotease, FLAG-ΔPH 2, and FLAG-ΔH 1 were expressed in 293T cells treated with 17-AAG. Proteins immunoprecipitated with anti-core, Hsp90 antibody were analyzed by Western blotting. 17-AAG-treated cell lysates were analyzed on Western blots, using the specific antibodies shown to the *right* of the panels. *Lane 1*, control; *lane 2*, 17-AAG (1 μM).

3*B*). However, when 50 nM 17-AAG was added to the cells at 3-day intervals for 15 days (*black squares*), the observed significant reduction in HCV RNA (by 3 log) was sustained from day 3 to day 15. We used trypan blue staining to check that long term treatment with 17-AAG did not induce cellular toxicity (Fig. 3*A*). Our results suggested that 17-AAG has the potential to safely induce long term suppression in HCV replication.

Reduced Expression of NS3 Protein in 17-AAG-treated HCV Replicon Cells—To investigate the mechanism by which 17-AAG inhibited HCV replication, we analyzed the expression of HCV core, E1, E2, NS3, NS4A, NS4B, NS5A, and NS5B proteins by Western blotting. NNC#2 cells treated with increasing doses of 17-AAG showed a marked reduction in the expression of NS3 (Fig. 4*A*) after 3 days, in common with the level of HCV RNA (Fig. 2*A*). However, levels of the other proteins were unchanged. This dose-dependent inhibition suggested that NS3 was more sensitive to 17-AAG than the other proteins. Similar effects on NS3 expression and RNA replication were seen in #50-1 cells treated with 17-AAG (Fig. 4*A*).

Another effect of 17-AAG treatment seen in these cells was an increase in Hsp70 expression and a slight increase in Hsp90 expression (Fig. 4*B*). The induction of Hsp70 expression suggested that Hsp90 inhibition by 17-AAG strongly activated HSF-1 (heat-shock transcription factor 1) (43). We also examined the levels of HCV core and NS5B protein expression in NNC#2 cells treated with 50 nM 17-AAG. Reduced levels of these proteins were seen in NNC#2 cells on day 6, and both HCV core and NS5B protein were undetectable on day 9 (Fig. 4*C*). To determine whether 17-AAG promoted the degradation of NS3, we next looked at the effect of 17-AAG on #50-1 cells in which proteasomal degradation was also inhibited. Although 17-AAG treatment still induced a reduction in the NS3 protein level in #50-1 cells (Fig. 4*D*), the degradation of NS3 was completely blocked in the presence of the proteasome inhibitor, MG132. This suggested that the pharmacological effect of 17-AAG was dependent on the proteasome system (44, 45).

Protein Folding in Hsp90-NS3 Interaction—To investigate the role of Hsp90 in HCV NS3 activation, the FLAG-NS3 protein was transfected into 293T cells, with or without 17-AAG, and the cell lysates were analyzed by Western blotting. The expression of NS3 from FLAG-NS3 was reduced in the presence of 17-AAG (Fig. 5*A*), suggesting that Hsp90 is involved in HCV NS3 degradation, possibly through a physical interaction.

We confirmed this specific interaction by immunoprecipitating 293T cell lysates with anti-FLAG antibody. This clearly showed that FLAG and Hsp90 co-precipitated, suggesting that NS3 was bound to the chaperone complex formed with Hsp90 (Fig. 5*B*). NS3 mutants lacking the protease and helicase regions were generated in order to identify the region responsible for the interaction with Hsp90 (Fig. 5*C*). FLAG-NS3, FLAG-NS3-Δhelicase, or FLAG-NS3-Δprotease were transfected into 293T cells, and anti-FLAG antibody immunoprecipitates were analyzed by Western blotting (Fig. 5*D*). Although FLAG-NS3-Δprotease was clearly co-immunoprecipitated with Hsp90, no protein band corresponding to FLAG-NS3-Δhelicase was detected (Fig. 5*D*), suggesting that the NS3 helicase region mediates binding to Hsp90. To confirm this finding, plasmids expressing different NS3 helicase mutants fused with FLAG (ΔPH 1, ΔPH 2, and ΔH 1) were constructed (Fig. 5*E*). Expressing these NS3 helicase mutants in 293T cells and analyzing their immunoprecipitates with anti-FLAG antibody by Western blotting showed that, although all of the NS3 helicase mutant proteins were immunoprecipitated by anti-FLAG-antibody, no Hsp90 was co-precipitated (Fig. 5*F*).

We also confirmed that the NS3 helicase region mediated the specific interaction with Hsp90 by transfecting FLAG-NS3 and FLAG-NS3 deletion mutants into 293T cells pretreated with 17-AAG (Fig. 5*G*). The proteins expressed by FLAG-NS3 and FLAG-NS3-Δprotease were degraded in cells pretreated with 17-AAG, whereas no degradation of the ΔPH 2 and ΔH 1 NS3 mutants lacking helicase regions was seen (Fig. 5*G*). Further, when pEF-core was expressed in 293T cells, core was unable to co-immunoprecipitate Hsp90, and no degradation of core protein was observed (Fig. 5*G*). Our data demonstrate that 17-AGG destabilizes several binding proteins (NS3 and NS3-Δprotease) to Hsp90 but stablilizes some nonbinding proteins (the ΔPH 2 and ΔH 1 NS3 mutants lacking helicase regions and core) to Hsp90. In previous reports (46), similar effects were observed when wild-type and mutated p53 were translated in the presence of geldanamycin. These results further supported the hypothesis that Hsp90 has a role in folding the NS3 helicase domain and that this has an important role in stabilizing the full-length NS3 protein. A protein complex that includes NS3 and Hsp90 is therefore implicated in the control of HCV replication.

DISCUSSION

The Hsp90 inhibitor, 17-AAG, is known to have highly selective effects on tumor cells that are a result of its high affinity for Hsp90 client oncoproteins, which are incorporated into the Hsp90-dependent multichaperone complex, thereby increasing their binding affinity for 17-AAG more than 100-fold (47). This high selectivity effectively minimizes the toxic side effects of 17-AAG so that it is a good candidate for clinical application, especially in treating neurodegenerative diseases. In this study, we observed the inhibitory effects of 17-AAG on the replication of an HCV subgenomic replicon that lacked NS2. On the other hand, Waxman *et al.* (37) demonstrated a role for Hsp90 in promoting the cleavage of HCV NS2/3 protein using NS2/3 translated in rabbit reticulocyte lysate and expressed in Jurkat cells. Because the replicon cells used in our study genetically lacked NS2, our results suggest that Hsp90 may directly interact with the NS3 protein in the HCV replicon.

In cell lines in which 17-AAG was a potent inhibitor of HCV replication, with IC_{50} values of 3–10 nM, we also found strong evidence that the association between HCV Hsp90 and NS3, but not other NS proteins, was the essential mechanism controlling the preferential degradation of NS3 after 17-AAG treatments. Furthermore, we showed that NS3 interacted with Hsp90 through the NS3 helicase domain. It was also clear that the expression of NS3 protein with helicase activity in 293T cells pretreated with 17-AAG was reduced, but the expression of NS3 mutants lacking the helicase regions (ΔPH 2 and ΔH 1) was not. The role of Hsp90 in achieving and/or stabilizing the NS3 protein was suggested by the fact that only 17-AGG bound to Hsp90 was capable of affecting NS3. The use of Hsp90 inhibitors represents a novel strategy for the development of anti-HCV therapies.

Acknowledgments—We are grateful to M. Sato, R. Tobita, and Y. Katumura for excellent technical assistance.

REFERENCES

1. Alter, H. J., Purcell, R. H., Shih, J. W., Melpolder, J. C., Houghton, M., Choo, Q. L., and Kuo, G. (1989) *N. Engl. J. Med.* **321,** 1494–1500
2. Choo, Q. L., Kuo, G., Weiner, A. J, Overby, L. R., Bradley, D. W., and Houghton, M. (1989) *Science* **244,** 359–362
3. McHutchison, J. G., Gordon, S. C., Schiff, E. R., Shiffman, M. L., Lee, W. M., Rustgi, V. K., Goodman, Z. D., Ling, M. H., Cort. S., and Albrecht, J. K. (1998) *N. Engl. J. Med.* **339,** 1485–1492
4. Glue, P., Rouzier-Panis, R., Raffanel, C., Sabo, R., Gupta, S. K., Salfi, M., Jacobs, S., and Clement, R. P. (2000) *Hepatology* **32,** 647–653
5. Saito, I., Miyamura, T., Ohbayashi, A., Harada, H., Katayama, T., Kikuchi, S., Watanabe, Y., Koi, S., Onji, M., and Ohtaet, Y. (1990) *Proc. Natl. Acad. Sci. U. S. A.* **87,** 6547–6549
6. Seeff, L. B. (1997) *Hepatology* **26,** 21S–28S
7. Bartenschlager, R., and Lohmann, V. (2001) *Antiviral Res.* **52,** 1–17
8. Taylor, D. R., Shi, S. T., Romano, P. R., Barber, G. N., and Lai, M. M. (1999) *Science* **285,** 107–110
9. Grakoui, A., Wychowski, C., Lin. C., Feinstone, S. M., and Rice, C. M. (1993) *J. Virol.* **67,** 1385–1395
10. Hijikata, M., Mizushima, H., Akagi, T., Mori, S., Kakiuchi, N., Kato, N., Tanaka, T., Kimura, K., and Shimotohno, K. (1993) *J. Virol.* **67,** 4665–4675
11. Grakoui, A., McCourt, D. W., Wychowski, C., Feinstone, S. M., and Rice, C. M. (1993) *Proc. Natl. Acad. Sci. U. S. A.* **90,** 10583–10587
12. Bartenschlager, R., Ahlborn-Laake, L., Mous, J., and Jacobsen, H. (1993) *J. Virol.* **67,** 3835–3844
13. Grakoui, A., McCourt, D. W., Wychowski, C., Feinstone, S. M., and Rice, C. M. (1993) *J. Virol.* **67,** 2832–2843
14. Bartenschlager, R., Lohmann, V., Wilkinson, T., and Koch, J. O. (1995) *J. Virol.* **69,** 7519–7528
15. Failla, C., Tomei, L., and De Francesco, F. (1995) *J. Virol.* **69,** 1769–1777
16. Lin, C., Thomson, J. A., and Rice, C. M. (1995) *J. Virol.* **69,** 4373–4380
17. Tanji, Y., Hijikata, M., Satoh, S., Kaneko, T., and Shimotohno, K. (1995) *J. Virol.* **69,** 1575–1581
18. Egger, D., Wolk, B., Gosert, R., Bianchi, L., Blum, H. E., Moradpour, D., and Bienz, K. (2002) *J. Virol.* **76,** 5974–5984
19. Gosert, R., Egger, D., Lohmann, V., Bartenschlager, R., Blum, H. E., Bienz, K., and Moradpour, D. (2003) *J. Virol.* **77,** 5487–5492
20. Blight, K. J., Kolykhalov, A. A., and Rice, C. M. (2000) *Science* **290,** 1972–1974
21. Guo, J. T., Bichko, V. V., and Seeger, C. (2001) *J. Virol.* **75,** 8516–8523
22. Krieger, N., Lohmann, V., and Bartenschlager, R. (2001) *J. Virol.* **75,** 4614–4624

23. Lohmann, V., Hoffmann, S., Herian, U., Penin, F., and Bartenschlager, R. (2003) *J. Virol.* **77,** 3007–3019
24. Behrens, S. E., Tomei, L., and De Francesco, R. (1996) *EMBO J.* **15,** 12–22
25. Lohmann, V., Korner, F., Herian, U., and Bartenschlager, R. (1997) *J. Virol.* **71,** 8416–8428
26. Friebe, P., and Bartenschlager, R. (2002) *J. Virol.* **76,** 5326–5338
27. Kolykhalov, A. A., Mihalik, K., Feinstone, S. M., and Rice, C. M. (2000) *J. Virol.* **74,** 2046–2051
28. Yanagi, M., St. Claire, M., Emerson, S. U., and Purcell Bukh, J. (1999) *Proc. Natl. Acad. Sci. U. S. A.* **96,** 2291–2295
29. Yi, M., and Lemon, S. M. (2003) *J. Virol.* **77,** 3557–3568
30. Picard, D. (2002) *Cell Mol. Life Sci.* **59,** 1640–1648
31. Wegele, H., Muller, L., and Buchner, J. (2004) *Rev. Physiol. Biochem. Pharmacol.* **151,** 1–44
32. Pratt, W. B., and Toft, D. O. (2003) *Exp. Biol. Med.* **228,** 111–133
33. Smith, D. F., Whitesell, L., and Katsanis, E. (1998) *Pharmacol. Rev.* **50,** 493–514
34. McClellan, A. J., and Frydaman, J (2001) *Nat. Cell Biol.* **3,** E1–E3
35. Grenert, J. P., Sullivan, W. P., Fadden, P., Haystead, T. A., Clark, J., Mimnaugh, E., Krutzsch, H., Ochel, H. J., Schulte, T. W., Sausville, E., Neckers, L. M., and Toft, D. O. (1997) *J. Biol. Chem.* **272,** 23843–23850
36. Supko, J. G., Hickman, R. L., Grever, M. R., and Malspeis, L. (1995) *Cancer Chemother. Pharmacol.* **36,** 305–315
37. Waxman, L., Whitney, M., Pollok, B. A., Kuo, L. C., and Darke, P. L. (2001) *Proc. Natl. Acad. Sci. U. S. A.* **98,** 13931–13935
38. Nakagawa, S., Umehara, T., Matsuda, C., Kuge, S., Sudoh, M., and Kohara, M. (2007) *Biochem. Biophys. Res. Commun.* **353,** 882–888
39. Okamoto, T., Nishimura, Y., Ichimura, T., Suzuki, K., Miyamura, T., Suzuki, T., Moriishi, K., and Matsuura, Y. (2006) *EMBO J.* **25,** 5015–5025
40. Kishine, H., Sugiyama, K., Hijikata, M., Kato, N., Takahashi, H., Noshi, T., Nio, Y., Hosaka, M., Miyanari, Y., and Shimotohno, K. (2002) *Biochem. Biophys. Res. Commun.* **290,** 993–999
41. Ishii, N., Watashi, K., Hishiki, T., Goto, K., Inoue, D., Hijikata, M., Wakita, T., Kato, N., and Shimotohno, K. (2006) *J. Virol.* **80,** 4510–4520
42. Takeuchi, T., Katsume, A., Tanaka, T., Abe, A., Inoue, K., Tsukiyama-kohara, K., Kawaguchi, R., Tanaka, S., and Kohara, M. (1999) *Gastroenterology* **11,** 636–642
43. Sittler, A., Lurz, R., Ueder, G., Priller, J., Lehrach, H., Hayer-Hartl, M. K., Hartl, F. U., and Wanker, E. E. (2001) *Hum. Mol. Genet.* **10,** 1307–1315
44. Bonvini, P., Dalla Rosa, H., Vignes, N., and Rosolen, A. (2004) *Cancer Res.* **64,** 3256–3264
45. Mimnaugh, E. G., Chavany, C., and Neckers, L. (1996) *J. Biol. Chem.* **271,** 22796–22801
46. Blagosklonny, M. V., Toretsky, J., Bohen, S., and Neckers L. (1996) *Proc. Natl. Acad. Sci. U. S. A.* **93,** 8379–8383
47. Kamal, A., Thao, L., Sensintaffar, J., Zhang, L., Boehm, M. F., Fritz, L. C., and Burrows, F. J. (2003) *Nature* **425,** 357–359

The EMBO Journal (2009) 28, 440–451 | © 2009 European Molecular Biology Organization | All Rights Reserved 0261-4189/09
www.embojournal.org

THE EMBO JOURNAL

Structure, interaction and real-time monitoring of the enzymatic reaction of wild-type APOBEC3G

Ayako Furukawa[1], Takashi Nagata[1], Akimasa Matsugami[1], Yuichirou Habu[2], Ryuichi Sugiyama[2], Fumiaki Hayashi[3], Naohiro Kobayashi[3], Shigeyuki Yokoyama[3,4], Hiroshi Takaku[2] and Masato Katahira[1,5,*]

[1]Supramolecular Biology, International Graduate School of Arts and Sciences, Yokohama City University, Yokohama, Japan, [2]Department of Life and Environmental Science and High Technology Research Center, Chiba Institute of Technology, Narashino, Japan, [3]Systems and Structural Biology Center, RIKEN, Yokohama, Japan, [4]Department of Biophysics and Biochemistry, Graduate School of Science, The University of Tokyo, Tokyo, Japan and [5]PRESTO, JST, Yokohama, Japan

Human APOBEC3G exhibits anti-human immunodeficiency virus-1 (HIV-1) activity by deaminating cytidines of the minus strand of HIV-1. Here, we report a solution structure of the C-terminal deaminase domain of wild-type APOBEC3G. The interaction with DNA was examined. Many differences in the interaction were found between the wild type and recently studied mutant APOBEC3Gs. The position of the substrate cytidine, together with that of a DNA chain, in the complex, was deduced. Interestingly, the deamination reaction of APOBEC3G was successfully monitored using NMR signals in real time. Real-time monitoring has revealed that the third cytidine of the d(CCCA) segment is deaminated at an early stage and that then the second one is deaminated at a late stage, the first one not being deaminated at all. This indicates that the deamination is carried out in a strict 3′→5′ order. Virus infectivity factor (Vif) of HIV-1 counteracts the anti-HIV-1 activity of APOBEC3G. The structure of the N-terminal domain of APOBEC3G, with which Vif interacts, was constructed with homology modelling. The structure implies the mechanism of species-specific sensitivity of APOBEC3G to Vif action.

The EMBO Journal (2009) **28**, 440–451. doi:10.1038/emboj.2008.290; Published online 15 January 2009
Subject Categories: structural biology
Keywords: APOBEC3G; cytidine deaminase; HIV; structure; Vif

Introduction

The apolipoprotein B messenger RNA-editing enzyme catalytic polypeptide (APOBEC)/activation-induced cytidine deaminase (AID) proteins are found in vertebrates and share the ability to mutate either DNA or RNA by deaminating cytidine to uridine (Rogozin *et al*, 2007). The APOPBEC1 deaminates and edits apolipoprotein B pre-mRNA (Navaratnam *et al*, 1993; Teng *et al*, 1993). AID deaminates immunoglobulin gene DNA, which is essential for the antigen-driven diversification of already rearranged immunoglobulin genes in the vertebrate adaptive immune system (Muramatsu *et al*, 1999). Human APOPBEC3G is expressed in spleen, testes, ovary and blood leukocytes, such as T lymphocytes and macrophages. APOBEC3G deaminates and modifies the newly synthesized cDNA minus strand of retroviruses such as the human immunodeficiency virus-1 (HIV-1) (Sheehy *et al*, 2002; Harris *et al*, 2003; Lecossier *et al*, 2003; Mangeat *et al*, 2003; Zhang *et al*, 2003; Beale *et al*, 2004; Greene, 2004; Harris and Liddament, 2004; Suspene *et al*, 2004; Yu *et al*, 2004; Esnault *et al*, 2005; Chelico *et al*, 2006). The modifications are supposed to induce degradation of the minus strand through action of uracil DNA glycosylase and apurinic–apyrimidinic endonuclease or the generation of G to A mutations upon synthesis of the plus strand, which may eliminate HIV-1 infectivity for virus infectivity factor (Vif)-deficient strains (Sheehy *et al*, 2002; Harris *et al*, 2003; Lecossier *et al*, 2003; Mangeat *et al*, 2003; Greene, 2004; Harris and Liddament, 2004; Esnault *et al*, 2005). Vif targets APOBEC3G for ubiquitination and proteasomal degradation, and thus abolishes the antiviral activity of APOBEC3G (Conticello *et al*, 2003; Marin *et al*, 2003; Yu *et al*, 2003; Mehle *et al*, 2004; Kobayashi *et al*, 2005).

In spite of the great attention to the APOBEC/AID protein family, the structural knowledge on this family is quite limited. The structure of APOBEC2 was reported last year (Prochnow *et al*, 2007), but APOBEC2 does not possess enzymatic activity. APOBEC3G is composed of 384 residues and possesses two consensus cytidine deaminase motifs of the zinc-finger type, His-X-Glu-X_{27-28}-Pro-Cys-X_2-Cys, in its N- and C-terminal domains (Harris and Liddament, 2004). It is known that the C-terminal deaminase domain is catalytically active, whereas the N-terminal one is not (Navarro *et al*, 2005). Recently, the solution structure of a mutant C-terminal deaminase domain, residues 198–384, was reported (Chen *et al*, 2008). To increase the solubility, mutation of five residues of the C-terminal domain was performed. Here, we present the solution structure of the wild-type C-terminal deaminase domain, residues 193–384, which possesses no mutation. Some difference in structure was found between the wild type and mutant deaminase domains of APOBEC3G. The mode of interaction with single-stranded DNA (ssDNA) was characterized by chemical shift perturbation analysis. Although the wild-type and mutant APOBEC3Gs share several features of the interactions, many differences in the interaction were also identified between them. The differences were supposed to be partly due to the introduction of the mutations themselves. The position of a substrate cytidine, and the position and polarity of an ssDNA chain in the complex were deduced from the results of analysis of the interaction. Very recently, the crystal structure of the C-terminal deaminase domain of APOBEC3G has been

*Corresponding author. Supramolecular Biology, International Graduate School of Arts and Sciences, Yokohama City University, 1-7-29 Suehiro-cho, Tsurumi-ku, Yokohama 230-0045, Japan. Tel.: +81 45 508 7213; Fax: +81 45 508 7361; E-mail: katahira@tsurumi.yokohama-cu.ac.jp

Received: 18 October 2008; accepted: 9 December 2088; published online: 15 January 2009

reported (Holden *et al*, 2008). The relation between our and their findings is also discussed.

Moreover, we succeeded for the first time in monitoring the deamination reaction in real-time using NMR signals. This method enabled us to address the dynamical aspects of the deamination reaction by APOBEC3G. Deamination in a very strict 3′→5′ order was detected for consecutive cytidine residues of ssDNA.

The N-terminal domain of APOBEC3G is required for encapsidation of APOBEC3G into virion (Cen *et al*, 2004; Harris and Liddament, 2004). It is also known that Vif of HIV-1 interacts with the N-terminal domain of APOBEC3G (Conticello *et al*, 2003; Harris and Liddament, 2004). The structure of the N-terminal domain has not been reported. The N- and C-terminal domains of APOBEC3G exhibit sequence homology. So, the structure of the N-terminal domain is constructed with homology modelling on the basis of the structure of the wild-type C-terminal domain. The constructed structure suggests the origin of species-specific sensitivity of APOBEC3G to Vif action.

Results

Structure of the wild-type deaminase domain of APOBEC3G

Figure 1A shows SDS–polyacrylamide gel electrophoresis of the purified deaminase domain of wild-type APOBEC3G. The purity was estimated to be over 99%. Figure 1B shows the ^{1}H–^{15}N HSQC spectrum of the deaminase domain of wild-type APOBEC3G. The HSQC peaks are sharp and well dispersed, which guarantees that the sample prepared with our procedure possesses the native structure, not being in an aggregated state, and is suitable for structure determination. Thus, it was found that wild-type APOBEC3G, instead of the mutant, could be used for the structure determination.

The structure of wild-type APOBEC3G was calculated on the basis of distance and dihedral angle constraints. The structure statistics are presented in Table I. The average pairwise r.m.s.d. between the 10 final structures as to the backbone atoms of the all secondary elements was 0.55 ± 0.110 Å. Figure 1C and D shows the structures of wild-type APOBEC3G. Wild-type APOBEC3G is composed of five β-strands, β1–β5, and five α-helices, α1–α5, which are arranged in the order of β1-β2/β2′-α1-β3-α2-β4-α3-β5-α4-α5. The second β-strand is interrupted and divided into two short β-strands, β2 and β2′.

In Figure 2, the structure of the wild-type APOBEC3G determined in solution by NMR (this study) is compared with the structure of the mutant carrying five substituted residues determined in solution by NMR (Chen *et al*, 2008), and also with the structure of the wild type determined for crystal by X-ray (Holden *et al*, 2008). The three structures are mostly similar to each other. An extra α-helical element, α0 (P199-F204), is formed for the wild type in solution (Figure 2A), but not for the mutant in solution (Figure 2B). The formation of α0 for the wild type in solution was

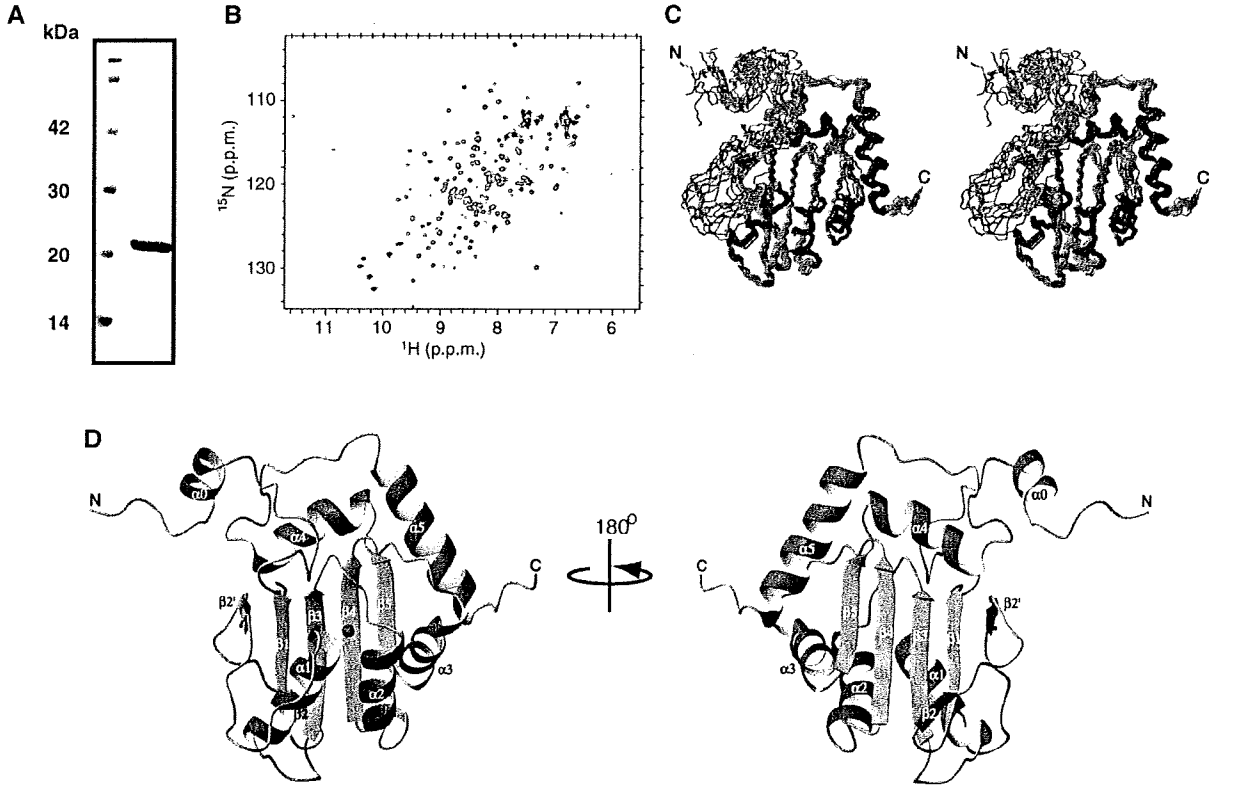

Figure 1 SDS–polyacrylamide gel electrophoresis, HSQC spectrum and structure of the deaminase domain of the wild-type APOBEC3G. (**A**) SDS–polyacrylamide gel electrophoresis of the purified APOBEC3G. (**B**) ^{1}H–^{15}N HSQC spectrum. (**C**) A stereo view of superposition of the main chains of 10 final structures. N and C indicate L193 and N384, respectively. α-helices and β-strands are coloured red and blue, respectively. (**D**) The main chain of a representative structure with the lowest energy. α-helices and β-strands are coloured red/yellow and blue, respectively.

supported by the secondary structure identification on the basis of chemical shifts of C^{α}, C^{β}, C′, N and H^{α} with either CSI (Wishart and Sykes, 1994) or TALOS (Cornilescu *et al*, 1999). α0 (P199-F206) is also present for the wild type in crystal (Figure 2C). The wild type is composed of either L193-N384 (this study) or M197-Q380 (Holden *et al*, 2008), and the mutant of D198-N384. The lack of α0 in the mutant may be due to the lack of several N-terminal residues. Because of the lack of long-range NOEs involving α0, the relative position of α0 as to the rest of APOBEC3G was poorly determined (Figure 1C). Therefore, it is hard to discuss the difference in the relative position of α0 between the wild-type APOPBEC3Gs in solution and crystal.

Table I NMR and refinement statistics for protein structures

	Protein
NMR distance and dihedral constraints	
Distance constraints	
Total NOE	2380
Intra-residue	1117
Inter-residue	1263
Sequential ($\|i-j\|=1$)	581
Medium range ($\|i-j\|<4$)	311
Long range ($\|i-j\|>5$)	371
Hydrogen bonds	112
Total dihedral angle restraints	
ϕ	131
ψ	131
Structure statistics	
Violations (mean and s.d.)	
Distance constraints (Å)	0.0779 ± 0.0008
Dihedral angle constraints (deg)	0.7545 ± 0.0703
Maximum dihedral angle violation (deg)	7.718
Maximum distance constraint violation (Å)	0.478
Deviations from idealized geometry	
Bond lengths (Å)	0.0044 ± 0.0001
Bond angles (deg)	0.6595 ± 0.0055
Impropers (deg)	0.4181 ± 0.0067
Average pairwise r.m.s.d. between 10 structures (Å)	
Heavy[a]	1.38 ± 0.22
Backbone[a]	0.71 ± 0.14
Heavy[b]	1.26 ± 0.20
Backbone[b]	0.55 ± 0.11
Ramachandran plot appearance	
Most favoured regions (%)	71.5
Additional allowed (%)	25.9
Generously allowed (%)	2.3
Disallowed regions (%)	0.2

[a]These calculations included residues 221–242 and 258–379.
[b]These calculations included residues 221–228, 231–232, 240–242, 258–269, 276–283, 291–300, 305–311, 322–331, 333–338, 340–350 and 364–379.

The second β-strand is interrupted and divided into two short β-strands for both the wild type and mutant in solution (Figure 2A and B). The second β-strand of the wild type in crystal is not divided but continuous, although a bulge exists in this β-strand (Figure 2C). Typical NOEs expected for a β-strand structure were not detected for the interrupted region. The secondary structure identification on the basis of chemical shifts of C^{α}, C^{β}, C′, N and H^{α} also suggests the interruption at the central 3–5 residues of the second β-strand, although a β-strand-like structure is implied for the other region of the strand. Thus, it is not likely that the continuous β-strand is stably formed in solution.

The mutation of either F202 or T203 of α0 to Ala causes the decrease of the activity of APOBEC3G (Supplementary data of Chen *et al*, 2008). Similarly, the mutation of W232, V233, L235, F241 or L242 of β2 to Lys and that of either W232, V233, L235 or L242 of β2 to Ala cause the decrease of the activity of APOBEC3G (Supplementary data of Chen *et al*, 2008). Therefore, the structural differences detected for α0 and β2 may have some functional relevance.

Binding of the wild-type deaminase domain to a ssDNA, as revealed by a gel retardation experiment

It was reported that minus strand deamination by APOBEC3G occurs preferentially at a CCCA sequence (Yu *et al*, 2004). 10-mer DNA, d(ATTCCCAATT), contains the CCCA sequence in the middle. Binding of the deaminase domain of the wild-type APOBEC3G to a short single-stranded 10-mer DNA was revealed by gel retardation experiments (Figure 3). To our best knowledge, this is the first demonstration by a gel retardation experiment that the deaminase domain can bind to a short ssDNA of only 10 residues, although the binding of full-length APOPBEC3G to another 10-mer DNA was demonstrated on the basis of the change in steady-state fluorescence

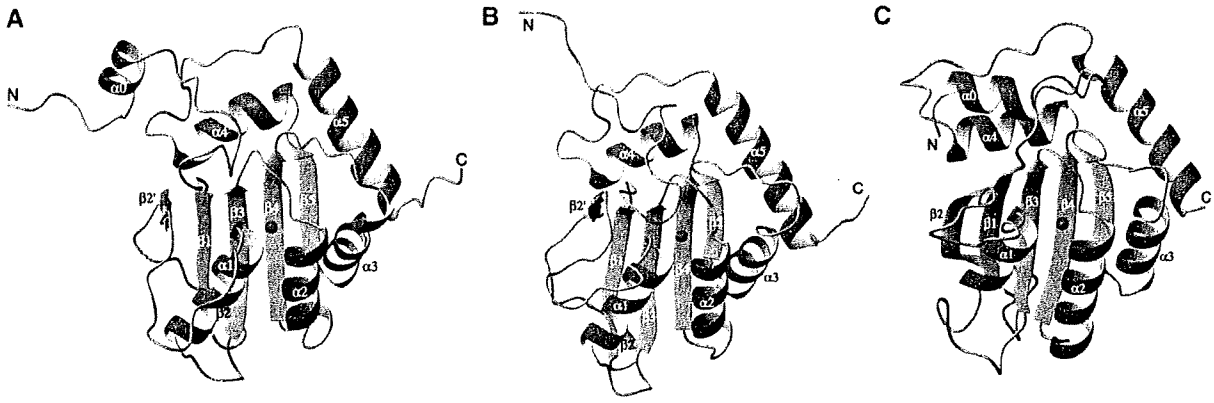

Figure 2 Comparison of the structures of the deaminase domain of APOBEC3G. (**A**) The wild type in solution by NMR (this study). (**B**) The mutant carrying five substitutions in solution by NMR (Chen *et al*, 2008). (**C**) The wild type in crystal by X-ray (Holden *et al*, 2008).

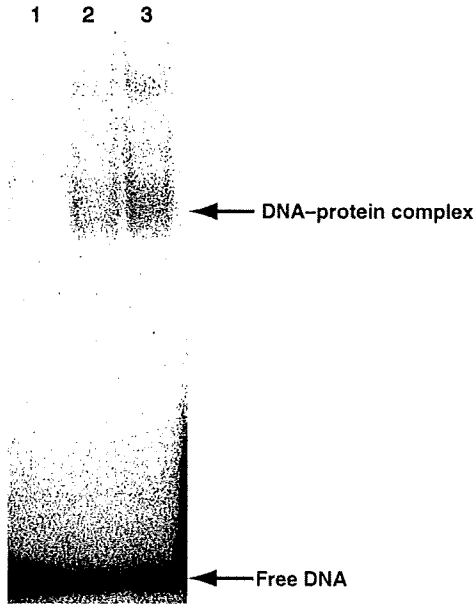

Figure 3 Gel retardation experiments indicating binding of the wild-type deaminase domain to a short ssDNA comprising 10 residues. ^{32}P-labelled 10-mer DNA (200 nM), d(ATTCCCAATT), was incubated with 0, 40 and 80 μM of the deaminase domain of the wild-type APOBEC3G (lanes 1–3). The mixtures were run on a polyacrylamide gel and then exposed.

depolarization of fluorescein-labelled DNA (Chelico *et al*, 2006). The apparent dissociation constant, K_d, was estimated to be ca. 130–190 μM, on the basis of the relative intensities of bands corresponding to either free DNA or the DNA–protein complex. K_d for the complex between the mutant deaminase domain and a 21-mer ssDNA was reported to be minimally 450 μM, on the basis of the results of a chemical shift perturbation experiment (Chen *et al*, 2008). Thus, the affinity of the wild type to 10-mer DNA is comparable or slightly higher than that of the mutant to 21-mer DNA. Therefore, 10-mer DNA was used for further analysis of the interaction using the chemical shift perturbation method.

The differences in the interaction of the deaminase domain with ssDNA between the wild-type and mutant APOBEC3Gs, as revealed by chemical shift perturbation

Figure 4A and C shows the chemical shift perturbations for the deaminase domain of the wild-type APOBEC3G on binding of ssDNA, d(ATTCCCAATT). For comparison, Figure 4B shows the chemical shift perturbations reported for the mutant deaminase domain on binding of 21-mer ssDNA (Chen *et al*, 2008). In general, perturbations detected for the wild-type APOBEC3G:10-mer DNA complex were larger than those for the mutant APOBEC3G:21-mer DNA complex: the maximum perturbation for the mutant was 0.03 p.p.m., whereas six residues exhibited perturbation of greater than 0.03 p.p.m. for the wild type. The larger perturbations could be partly due to the higher oligonucleotide ratio to APOBEC3G (an APOBEC3G:DNA ratio is 1:10 for our case, whereas the ratio is 1:4 for Chen *et al*) and/or the use of the wild-type APOBEC3G. It is expected that the mode of the interaction may be deduced more precisely with the pronounced perturbation data obtained here.

It is known that E259 is a catalytic residue for the deamination reaction (Mangeat *et al*, 2003; Shindo *et al*, 2003; Navarro *et al*, 2005). Chemical shift perturbation, including a decrease in the intensity of a correlation peak, was detected for residues surrounding E259. Perturbations were seen for the residues of the loop between α0 and β1 (an α0–β1 loop) (N208 and R215), those of a β2′–α1 loop (C243, A246, E254, R256 and H257), those of α1 (L260, C261, F262, L263, V265 and I266), those of β4 (V305 and S306), those of a β4–α3 loop (D316 and G319), that of β5 (I337), that of α4 (D348) and those of an α4–α5 loop (V351, D352 and D362) (Figure 4A). Similar perturbations were observed for the mutant APOBEC3G for the same segments (Figure 4B). On the other hand, the perturbations observed for the following segments are specific to the wild type, not being observed for the mutant: a β2–β2′ loop (R238), β2′ (G240 and L242), an α1–β3 loop (L271, D272, D274 and Q275), β3 (R278), a β3–α2 loop (T283 and S284) and the N-terminal region including α0 (S196, D198 and F204) (Figure 4A).

Differences in chemical shift perturbation between the wild-type and mutant APOBEC3Gs may partly be attributed to the mutations themselves. Perturbations for R238, G240, L242 and C243 were observed for the wild type, but not for the mutant (Figure 4A and B). These residues are close to C243, so the mutation of Cys243 to Ala may be responsible for the decrease in the perturbations for the mutant. Similarly, perturbations for G319 and Q322 were exclusively observed for the wild type (Figure 4A and B). The mutation of close Cys321 to Ala may be responsible for the decrease in the perturbations for the mutant. Moreover, perturbations were observed for the residues of α0 and those close to α0 for the wild type, whereas perturbations were not observed for the corresponding N-terminal region of the mutant (Figure 4A and B). As described previously, the mutation of either F202 or T203 of α0 causes the decrease of the activity of APOBEC3G. So, the interaction involving α0 may be meaningful. From these points of view, it is critical to have perturbation data on the wild-type APOBEC3G to deduce the interaction correctly.

Occurrence of the deamination reaction in an NMR tube

Figure 5A shows the pyrimidine (either cytidine or uridine residues) H5–C5 region of the ^{1}H–^{13}C HSQC spectrum of 10-mer DNA, d(A1T2T3C4C5C6A7A8T9T10). Three peaks corresponding to the C4, C5 and C6 residues of 10-mer DNA can be seen. It should be noted that the intensity of the left peak is two times greater than that of the right peak, and that the two signals overlap on the left peak. Figure 5B shows the same region of the 10-mer DNA obtained 24 h after the addition of the wild-type deaminase domain to the NMR tube, the molar ratio of DNA 10-mer:deaminase domain being 10:1. Two new peaks have appeared in Figure 5B, whereas one peak remains at the original position. The ^{13}C chemical shift values of the two new peaks imply that these peaks originate from uridine residues. This suggests that the deamination reaction occurred in the NMR tube.

It was reported that 5′-CC-3′ is the consensus sequence for deamination by APOBEC3G, where C is the site of the deamination (Beale *et al*, 2004). Therefore, there are three possible patterns of deamination for the C4C5C6 segment of 10-mer DNA, C4C5U6, C4U5C6 and C4U5U6. It was also reported that the third cytidine of the CCCA sequence,

underlined, is preferably deaminated by APOBEC3G (Yu *et al*, 2004; Chelico *et al*, 2006) and that the second cytidine is also deaminated to some extent (Chelico *et al*, 2006). To confirm the occurrence of the deamination, HSQC spectra of three mutant 10-mer DNAs in which the C4C5C6 segment was mutated to either C4C5U6, C4U5U6 or C4U5C6 were recorded for reference (Figure 5C–E). Then, it was found that the HSQC spectrum obtained 24 h after the addition of the wild-type deaminase domain (Figure 5B) was the same as that of the mutant 10-mer DNA with the C4U5U6 segment (Figure 5D).

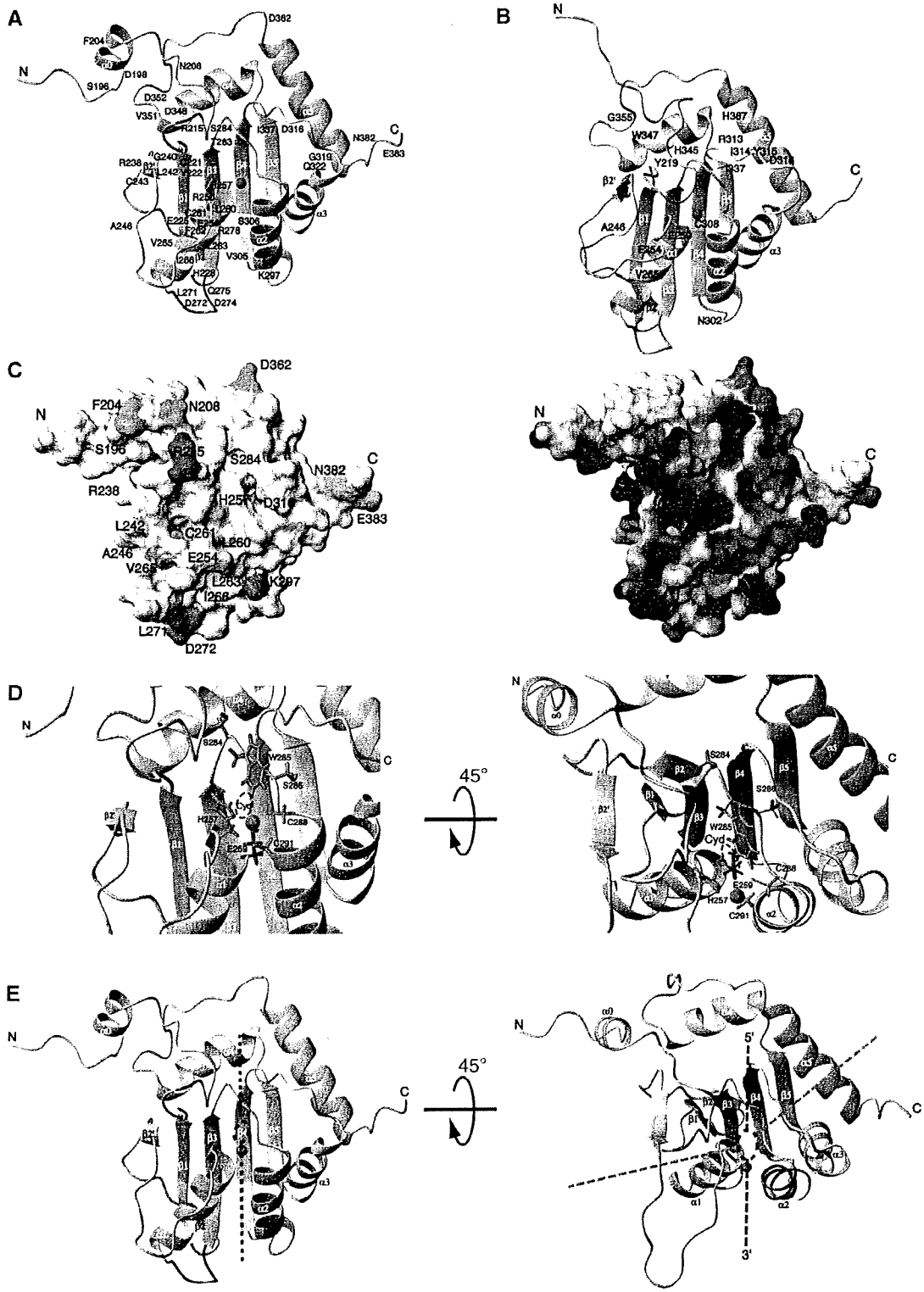

This clearly demonstrates that the deamination reaction by the wild-type deaminase domain actually occurred for C5 and C6 residues in the NMR tube.

Assignment of the H5–C5 correlation peaks for the U6 and U5 residues was performed in a straightforward way from the spectra of the mutant 10-mer DNAs with the C4C5U6 and C4U5C6 segments, respectively (Figure 5C and E), together with those for the C4, C5 and C6 residues. The assignments made are indicated in Figure 5.

Strictly regulated deamination of consecutive cytidine residues in a 3′→5′ order, as revealed by real-time monitoring of the reaction using NMR signals

Figure 6A–E shows the time chase of the ^{1}H NMR spectra of 10-mer DNA after the addition of the wild-type deaminase domain. For reference, ^{1}H NMR spectra of the three mutant 10-mer DNAs are also shown with the H5 assignments of the U5 and U6 residues. The H5 peak of the U6 residue is present in the spectrum recorded 30 min after the addition of the deaminase domain (Figure 6B). Generally, the H5 peak of a uridine residue is a doublet due to a $^{3}J_{H5H6}$ coupling. The intensity is comparable to that seen in the spectrum recorded 24 h after the addition. This indicates that the conversion of a C6 residue to a U6 residue through deamination by the wild-type deaminase domain has been almost completely accomplished within 30 min. The intensity of the H5 peak of the U5 residue is very weak in Figure 6B, but the intensity gradually increases (Figure 6C), becomes roughly half of the final intensity level in 4.5 h (Figure 6D), and finally reaches the same level as that of the U6 residue (Figure 6E). These results indicate that deamination occurs almost exclusively for the C6 residue at an early stage and that then deamination occurs for the C5 residue with a much slower reaction rate. Not only the C6 residue but also the C5 one is fully converted to a uridine residue at the end of the reaction. This is the first report that a strictly regulated deaminase reaction of consecutive cytidine residues in a 3′→5′ order can be directly monitored in real-time using NMR signals.

It was noted that the H5 peak of the U6 residue is a doublet at an early stage (Figure 6B), next becomes a triplet at a middle stage (Figure 6D) and finally becomes a doublet again (Figure 6E). It was found that the H5 doublet of the U6 residue of the C4U5U6 segment appears slightly in a downfield region compared with that of the C4C5U6 segment: the position of the right half of the former doublet almost coincides with that of the left half of the latter doublet. Therefore, the H5 peak of the U6 residue becomes a triplet when roughly half of the C5 residue has been converted to U5 in the course of the reaction (Figure 6D).

The structure of the N-terminal domain of APOBEC3G constructed on the basis of the structure of the C-terminal domain

The N- and C-terminal domains of human APOBEC3G exhibit the sequence homology, the sequence identity and similarity being 36 and 54%, respectively. So, the structure of the N-terminal domain of human APOBEC3G (residues 10–192) was constructed with homology modelling on the basis of the structure of the C-terminal wild-type deaminase domain of human APOBEC3G (Figure 7A), using the program MODELLER 9v3 (Marti-Renom *et al*, 2000). To address the origin of species-specific sensitivity of APOBEC3G to Vif action, which is discussed below, the structure of the N-terminal domain of APOBEC3G of African green monkey (AGM) (residues 10–192) is also constructed in the same way (Figure 7B). The sequence identity and similarity between the N-terminal domain of AGM APOBEC3G and the C-terminal domain of human APOBEC3G are 38 and 53%, respectively. As discussed below, the residue at the position 128 governs the species-specific sensitivity of APOBEC3G to Vif action, and is indicated in Figure 7A and B. Surface potentials of the N-terminal domains of human and AGM APOBEC3Gs are shown in Figure 7C and D, respectively, the residue at the position 128 being indicated with a circle. D128 of human APOBEC3G and K128 of AGM APOBEC3G locate at the surface, which is suitable for these residues to interact with Vif.

Discussion

We found that the deamination reaction occurs in an NMR tube during a titration experiment and that the pH value of the solution in the NMR tube increases, probably due to the release of NH_3 as a result of the reaction (Harris and Liddament, 2004). The H^N and N chemical shift values of some residues were sensitive to the change in pH. In particular, we noticed that the chemical shift values of His residues and residues close to the His residues were sensitive to the pH change. Therefore, at the end of the titration, we adjusted the pH of the protein–DNA complex solution to that of the initial protein alone solution. After the adjustment, the HSQC spectrum of the complex was recorded and the chemical shift values of the complex were obtained. It should be noted that if the adjustment is not carried out, false perturbations originating from the pH change, which do not reflect the interaction with DNA, would be mixed up. For example, although H345 exhibited an apparent chemical shift perturbation of greater than 0.02 p.p.m., the perturbation diminished after adjustment of the pH. Perturbation was reported for H345 of the mutant APOBEC3G (Chen *et al*, 2008). There is a

Figure 4 Mapping of chemical shift perturbations upon binding of DNA, surface electrostatic potential and proposed position of a substrate cytidine. (**A**) Chemical shift perturbations observed for the wild-type deaminase domain upon binding of 10-mer DNA. The residues exhibiting combined chemical shift perturbations as to H^N and N of >0.03 p.p.m. and 0.02–0.03 p.p.m. are coloured red and yellow, respectively. The residues whose ^{1}H–^{15}N correlation peaks either disappeared or became notably weak, the relative intensity in a free state to that in a complex state being greater than 1.2, are coloured blue. (**B**) Chemical shift perturbations observed for the mutant deaminase domain upon binding of 21-mer DNA. The residues exhibiting combined chemical shift perturbations of >0.03 p.p.m. and 0.02–0.03 p.p.m. are coloured red and yellow, respectively. The structure and perturbation data reported for the mutant deaminase domain (Chen *et al*, 2008) were used to make this figure. (**C**) Left, the perturbations for the wild-type deaminase domain mapped on the surface representation; right, positive and negative surface potentials of the wild-type deaminase domain represented in blue and red, respectively. (**D**) A close-up of the deduced key interactive region of the wild-type APOBEC3G deaminase domain, with the proposed position of a substrate cytidine indicated by a dashed circle, viewed from two different angles. (**E**) Three possible positions of ssDNA relative to the APOBEC3G deaminase domain. Right, the position proposed by Chen *et al*, 2008 (dashed vertical line in blue) and that by Holden *et al*, 2008 (dashed kinked horizontal line in green); left, the third possible position.

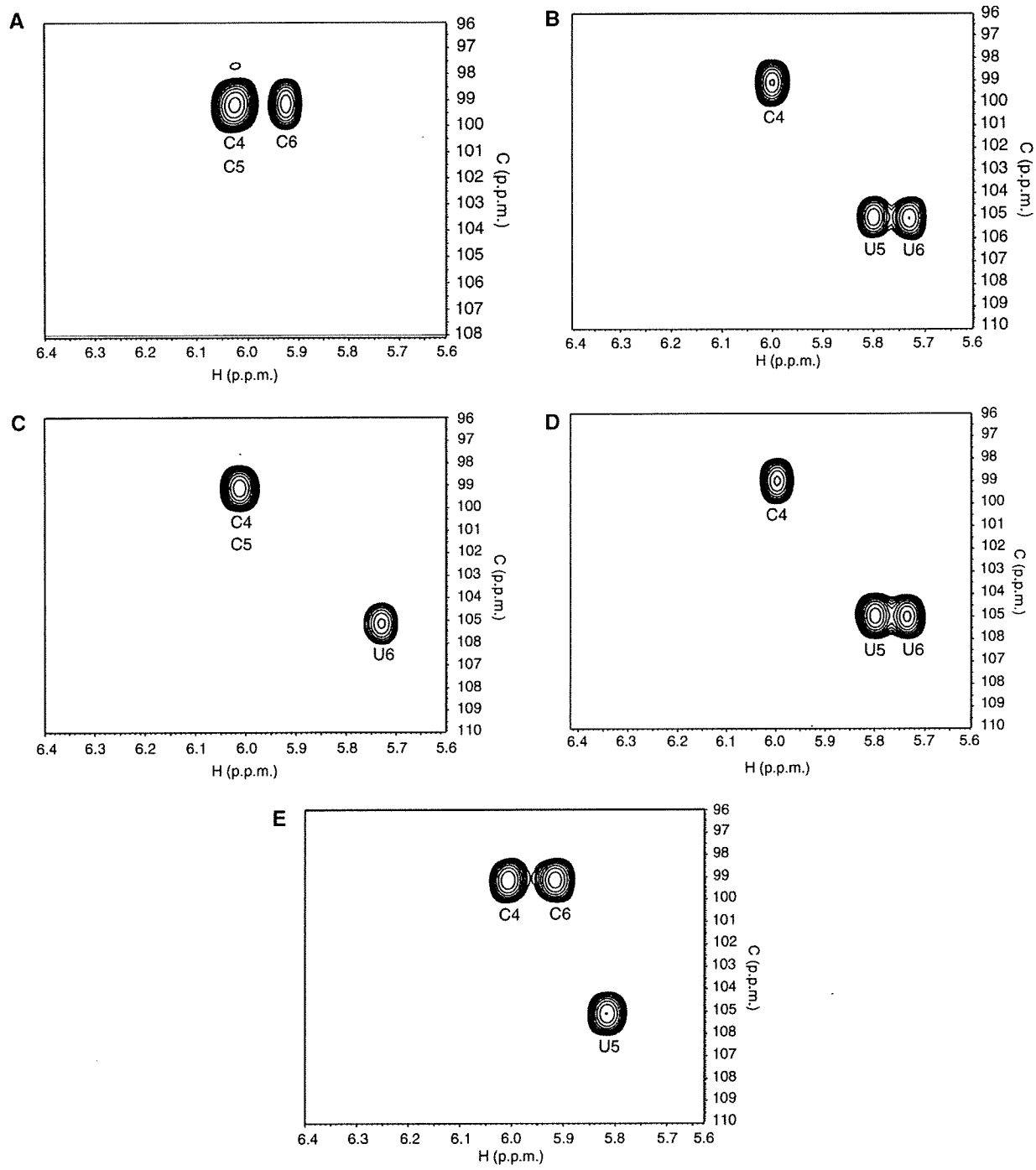

Figure 5 $^{1}H-^{13}C$ HSQC spectra indicating cytidine to uridine conversion for 10-mer DNA through the deamination reaction in an NMR tube. The pyrimidine (either cytidine or uridine residues) H5–C5 region of the $^{1}H-^{13}C$ HSQC spectrum of 10-mer DNA, d(ATTCCCAATT) (**A**), and that recorded 24 h after the addition of the wild-type deaminase domain to the NMR tube (**B**). The same regions of mutant 10-mer DNAs with the C4C5U6 (**C**), C4U5U6 (**D**) and C4U5C6 (**E**) segments, respectively, for reference.

possibility that this perturbation may have originated just from the pH change. In this sense, our perturbation data are supposed to be more adequate for accurately characterizing the interaction.

It was reported that APOBEC3G binds to any kind of ssDNA of larger than 9 nt with essentially the same affinity even in the absence of a cytidine (Chelico *et al*, 2006). Therefore, binding of the deaminase domain to 10-mer DNA can be expected even after the complete conversion of cytidines to uridines through deamination in an NMR tube. Thus, the interaction of the deaminase domain with 10-mer DNA can be examined with our method.

Among perturbations observed for various residues, the following are of particular interest. First, intensive perturba-

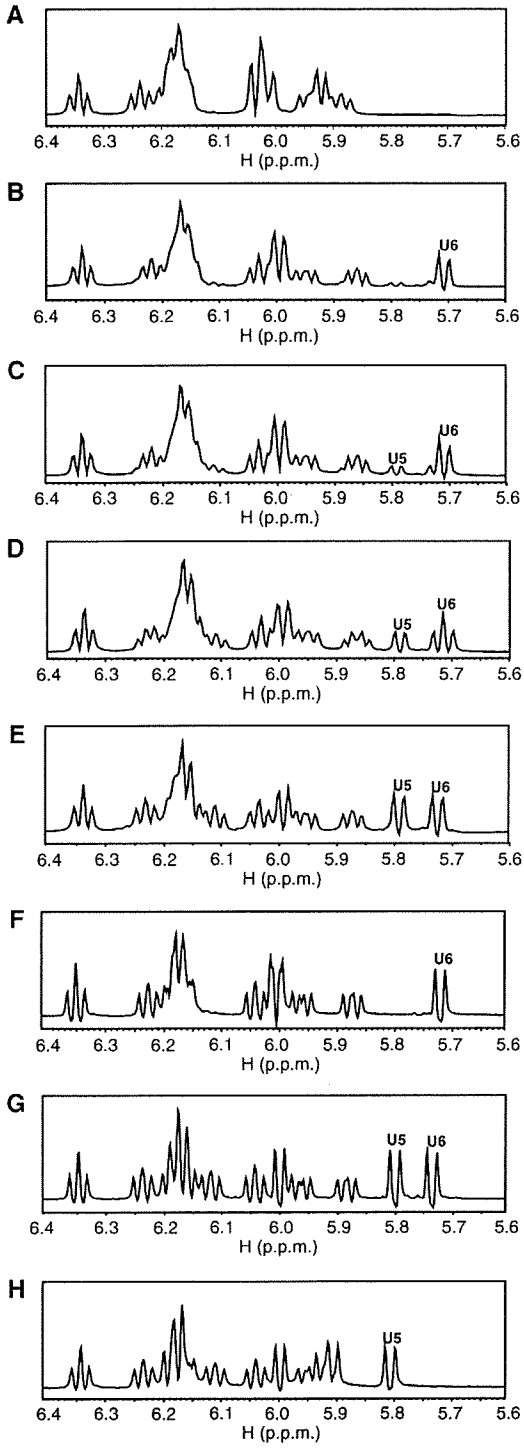

Figure 6 Time chase of ^{1}H NMR spectra indicating deamination of two cytidine residues in a strict 3′→5′ order. ^{1}H NMR spectrum of 10-mer DNA (**A**), and ones recorded 0.5 h (**B**), 1.5 h (**C**), 4.5 h (**D**) and 24 h (**E**) after the addition of the wild-type deaminase domain to the NMR tube. ^{1}H NMR spectra of mutant 10-mer DNAs with the C4C5U6 (**F**), C4U5U6 (**G**) and C4U5C6 (**H**) segments, respectively, for reference.

tions were observed for the following residues that are located close to the catalytic residue, E259; E254, R256, H257, L260, C261, F262 and L263 (Figure 4A). This implies that the substrate cytidine residue is positioned close to the catalytic residue in the APOBEC3G:ssDNA complex. In the crystal structures of *Escherichia coli* and mouse cytidine deaminases, a substrate cytidine is located close to the zinc-coordinating His residue (Xiang *et al*, 1997; Teh *et al*, 2006). On the basis of these structures, an APOBEC3G:ssDNA complex model was proposed in which the substrate cytidine is positioned close to the zinc-coordinating H257 residue (Chen *et al*, 2008). The perturbation observed for H257 of the wild type is consistent with this model. On the other hand, for the mutant, although perturbation was observed for E259, intensive perturbations for the residues around E259, including H257, were not seen (Figure 4B), which does not fit the model.

The S284-W285-S286 motif is conserved among DNA deaminases including APOBEC3G (Rogozin *et al*, 2007). Perturbations were observed for T283 and S284 for the wild type (Figure 4A). This implies that the substrate cytidine residue is positioned close to the conserved residues. In the proposed model mentioned above, W285 is located close to the substrate cytidine (Chen *et al*, 2008). The perturbation data for the wild type are consistent with this model. On the other hand, for the mutant, perturbation was not observed for the residues located close to the conserved residues (Figure 4B), which does not fit the model.

The surface potential of the wild-type deaminase domain is presented at the right of Figure 4C. The residues mentioned above, that is, those positioned close to E259 and S284-W285-S286, are located in a positively charged area, which is suitable for negatively charged ssDNA to interact with these residues. The chemical shift perturbation data and electrostatic features strongly suggest that this area is a key interactive region. A close-up of this area is shown in Figure 4D. The substrate cytidine is supposed to be positioned close to catalytic E259, conserved S284-W285-S286, and zinc-coordinating H257, as indicated by the dashed circle.

The position and polarity of the main chain of ssDNA in the complex with the deaminase domain were proposed on the basis of the results of analysis of the mutant APOBEC3G (Chen *et al*, 2008), as shown to the right of Figure 4E by a dashed vertical line in black. The model was constructed to have a similar main chain trace to that observed in the adenosine deaminase TadA:RNA complex (Losey *et al*, 2006). The main chain of ssDNA is located close to the area composed of the C-terminal regions of β3, β4 and β5, and the N-terminal regions of α1 and α2. The 3′ region of the main chain takes off and does not contact the deaminase domain.

Alternative model as to the position of the main chain of ssDNA has been proposed very recently (Holden *et al*, 2008), as shown to the right of Figure 4E by a dashed kinked horizontal line in green. The model is constructed on the basis of the crystal structure and mutational data. It is suggested that two active centre (AC) loops, AC loops 1 and 3, are important for binding of DNA. AC loop 1 connects α0 and β1, and AC loop 3 does β2′ and α1. For our solution structure, convergence is poor for these loops (Figure 1C). This may be due to either intrinsic flexibility of these loops or accidental lack of sufficient structural constraints for them. It is discussed that N244 and H257 of AC loop 3 are structurally conserved among crystals of Zn deaminases and may be involved in binding of the substrate cytidine (Holden *et al*, 2008). We observed the perturbations on binding of DNA for

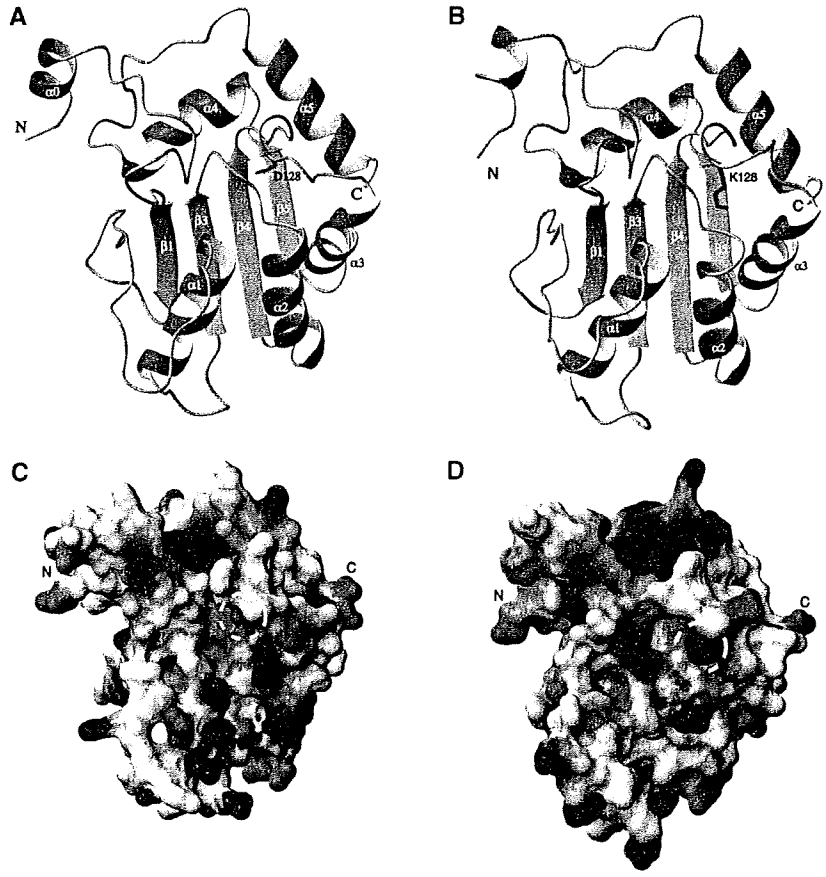

Figure 7 The structures of the N-terminal domains (residues 10–192) that interact with Vif. The structures of the N-terminal domains of human (**A**) and African green monkey (**B**) APOBEC3Gs, constructed with homology modelling on the basis of the structure of the C-terminal deaminase domain of human APOBEC3G. The surface potentials of the N-terminal domains of human (**C**) and African green monkey (**D**) APOBEC3Gs. The residue at the position 128 is indicated with a dashed circle.

C243 and A246, which are located close to N244, and for H257 and neighbouring R256 (Figure 4A), which may be related to their suggestion. It was also discussed that D316 and D317 may be important for positioning the substrate so that the third cytidine of the CCC sequence is most likely to be deaminated. We observed the perturbation on binding of DNA for D316 (Figure 4A), which may be related to their suggestion.

The results of analysis of the wild-type APOBEC3G in solution suggest the third model shown at the left of Figure 4E. For the wild type in solution, large chemical shift perturbations were observed for L271, D272, D274, Q275 and K297, together with medium perturbations for V305 and S306, whereas these were not observed for the mutant (Figure 4A and B). These perturbation data suggest that in the complex with the wild-type deaminase, ssDNA may go along α1 and α2 and that one end of the main chain of ssDNA is located close to the area composed of the N-terminal regions of β3 and β4, and the C-terminal regions of α1 and α2, as shown at the left of Figure 4E. The mutation of L271 to Ala causes the decrease in the activity of APOBEC3G (Supplementary data of Chen *et al*, 2008), which is consistent with our model in which L271 is supposed to mediate substrate contact. Nonetheless, it seems to us fair to say that at this moment we cannot select one of these possible positions on the basis of currently available information. We do not exclude the possibility that two or even three models are coexisting in solution.

It was found that deamination of ssDNA by APOBEC3G occurs preferentially at the CCCA sequence (Yu *et al*, 2004; Chelico *et al*, 2006). The third cytidine residue, underlined, is converted to a uridine residue through deamination. Some deamination of the second cytidine residue was also detected after an extended reaction time, although experimental data for and detailed features of the deamination of the second cytidine residue, such as the reaction rate and yield, were not provided (Chelico *et al*, 2006). Here, we have succeeded for the first time to monitor the deamination reaction in real-time by means of NMR signals. First, it was revealed by the NMR spectra that the second and third cytidine residues, C5 and C6, of the C4C5C6A7 sequence of 10-mer DNA are fully deaminated and converted to uridine residues, U5 and U6, 24 h after the addition of the wild-type deaminase domain, whereas the first cytidine residue, C4, is not deaminated at all (Figure 5). Second, the time course of the deamination reaction was monitored and chased in real-time using NMR signals. Then, it was revealed that the deamination of the third cytidine residue, C6, and the resultant appearance of the signal of the generated uridine residue, U6, occur at a very early stage of the time course, that is, within 30 min after the

start of the reaction (Figure 6B). In contrast, it was found that the deamination of the second cytidine residue, C5, and the resultant appearance of the signal of the generated uridine residue, U5, occur at a very late stage of the time course. The reaction is accomplished between 4.5 and 24 h, probably around 10 h, after the start of the reaction (Figure 6B–E). Virtually, it looks as if the deamination of the C5 residue starts after accomplishment of deamination of the C6 residue. Finally, both the C5 and C6 residues are fully deaminated and converted to uridine residues. Thus, the detailed time course of the deamination reaction of consecutive cytidine residues was visualized by means of NMR signals. The monitoring demonstrated that the deamination reaction occurs in a strict 3′→5′ order.

It was reported that when there are two CCCA sequences in one ssDNA, the deamination of the third cytidine residue by APOBEC3G occurs more frequently for the CCCA sequence located closer to the 5′ end. On the basis of this finding, it was concluded that APOBEC3G exerts an effect on multiple CCCA sequences processively with 3′→5′ directionality along ssDNA (Chelico *et al*, 2006). What we found here is the order of the reaction within one CCCA sequence. Therefore, the two findings regard different phenomena but may be linked to each other in the sense of 3′→5′ directionality/order.

The method of real-time monitoring of the enzymatic reaction with NMR signals has been established in this work, and its usefulness to address the dynamical aspects of the reaction is demonstrated. This method can be further applied in future to study unique features of APOBEC3G such as 3′→5′ directionality and processivity (Chelico *et al*, 2006). This method could also be applied to other enzymatic systems.

A C→U conversion through deamination in the minus strand causes a G→A mutation in the plus strand. Deamination of the third cytidine of a CCCA sequence in the minus strand results in the generation of a TAGG sequence in the plus strand, which contains a stop codon, TAG. Deamination of both the second and third cytidines of the CCCA sequence in the minus strand results in the generation of a TAAG sequence in the plus strand, which contains another stop codon, TAA. It is supposed that the anti-HIV activity of APOBEC3G is partially due to the generation of the stop codon through deamination and the resultant premature termination of viral open reading frames (Yu *et al*, 2004). APOBEC3G searches for the target sequence processively with 3′→5′ directionality through sliding and jumping after accomplishment of the deamination at the first target sequence (Chelico *et al*, 2006). Our results indicate that the deamination of the second cytidine residue of the CCCA sequence occurs at a rather later stage of the reaction time course. When the third cytidine residue of the CCCA sequence is already deaminated, further deamination of the second cytidine residue does not increase the number of stop codons, whereas deamination of the third cytidine residue of the other CCCA sequence does increase the number of stop codons. Therefore, it is reasonable that the deamination of the second cytidine residue of the CCCA sequence is carried out only at a later stage of the reaction time course in terms of the maximization of the anti-HIV activity of APOBEC3G through the generation of the stop codons.

Gag and *nef* initiation codons are mutated in 60 and 90% of Δ*vif* hu-APOBEC3G$^+$ reverse transcripts, respectively (Yu *et al*, 2004). The ATG initiation codons of *gag* and *nef* are followed by a G, forming a ATGG sequence. The minus strand of ATGG is CCAT. To mutate the initiation codon, deamination should occur at the cytidine residue next to an adenosine residue, not at the other cytidine residue. The phenomenon that the cytidine residue closest to the adenosine residue is preferably deaminated among three cytidine residues of the CCCA sequence may have been selected during evolution to effectively mutate the initiation codon and to maximize the anti-HIV activity of APOBEC3G.

APOBEC3G orthologues from several species are active against a broad range of retroviruses. For example, Vif-defective HIV-1 is blocked by APOPBEC3Gs from human, AGM and mouse (Mariani *et al*, 2003). Anti-HIV-1 activity of human APOBEC3G is counteracted by Vif of HIV-1 (Conticello *et al*, 2003; Yu *et al*, 2003; Mehle *et al*, 2004; Kobayashi *et al*, 2005). A far greater degree of specificity is found in the Vif sensitivity. For example, Vif of HIV-1 effectively counteracts human APOBEC3G but not APOBEC3G of AGM. Conversely, Vif of simian immunodeficiency virus (SIV) for AGM counteracts APOBEC3G of AGM but not human APOBEC3G (Mariani *et al*, 2003). Then, it was found that a single amino acid at the position 128 of human and AGM APOBEC3Gs governs the species-specific sensitivity of these proteins to Vif-mediated inhibition (Mangeat *et al*, 2004). The amino acid at the position 128 is Asp for human APOBEC3G and Lys for AGM APOBC3G, respectively. It was demonstrated that human APOBEC3G$_{D128K}$, in which Asp128 of human APOBEC3G was replaced by Lys, exhibited the same Vif sensitivity pattern as AGM APOBEC3G, as it became resistant to Vif of HIV-1, but was effectively blocked by Vif of SIV$_{AGM}$. Conversely, AGM APOBEC3G$_{K128D}$, in which Lys128 of AGM APOBEC3G was replaced by Asp, acquired the HIV-1 Vif susceptibility (Mangeat *et al*, 2004). It was further demonstrated that the phenotype correlates with the ability of Vif to bind APOBEC3G and interfere with its incorporation into virion (Mangeat *et al*, 2004).

The N-terminal domain of APOBEC3G is responsible for the binding to Vif (Conticello *et al*, 2003; Harris and Liddament, 2004) and the residue at the position 128 locates in this domain. The structures of the N-terminal domains of human and AGM APOBEC3Gs constructed with homology modelling have given the implication on the mechanism of species-specific sensitivity of APOBEC3G to Vif action. D128 of human APOBEC3G and K128 of AGM APOBEC3G are found to locate at the surface (Figure 7A and B), which would allow them to interact with Vif. It is noted that the surface potential is quite different around at the position 128 between human and AGM APOBEC3Gs, due to intrinsic difference in charge between Asp and Lys residues (Figure 7C and D). It is supposed that this difference in the surface potential is recognized by Vifs of either HIV-1 or SIV$_{AGM}$, which results in the species-specific sensitivity of APOBEC3G to Vif action. When D128 of human APOBEC3G is replaced by a Lys residue, the surface potential around at the position 128 becomes more similar to that of AGM APOBEC3G (data not shown), which also supports our idea.

Materials and methods

Preparation of wild-type APOBEC3G and DNA oligomers

DNA encoding the cytidine deaminase domain of wild-type APOBEC3G (193–384) was cloned into a pET15b expression vector with an N-terminal hexahistidine (His_6)-affinity tag and a thrombin cleavage site (Novagen). *E. coli* BL21(DE3/RIL) cells (Stratagene) were transformed with the vector and grown in 1 l of M9 minimal medium containing ^{13}C-labelled D-glucose and $^{15}NH_4Cl$ as the sole carbon and nitrogen sources, respectively, to an optical density at 600 nm of 0.6. Protein expression was induced with 1 mM IPTG at 37°C, and the cultures were harvested 5 h after induction by centrifugation (3000 *g*) for 20 min at 4°C. The cells were lysed by sonication in lysis buffer (20 mM Tris–HCl (pH 7.5) and 150 mM NaCl). The insoluble fraction was removed by centrifugation (16 000 *g*) for 20 min at 4°C. The soluble fraction was loaded onto a Ni Sepharose resin column (GE Healthcare), washed with a solution comprising 20 mM Tris–HCl (pH 7.5), 500 mM NaCl, 30 mM imidazole and eluted with an imidazole gradient of 30–500 mM. The His_6 tag was cleaved using 50 U of thrombin protease (GE Healthcare) in 20 mM Tris–HCl (pH 7.5), 500 mM NaCl, 10 μM $ZnCl_2$ and 5 mM DTT at 25°C overnight. After removal of thrombin with benzamidine-Sepharose resin (GE Healthcare), the solution was loaded onto a Ni Sepharose resin column again, washed with a solution comprising 20 mM Tris–HCl (pH 7.5), 500 mM NaCl, 30 mM imidazole, 10 μM $ZnCl_2$ and 5 mM DTT, and eluted with an imidazole gradient of 30–500 mM. The eluate was dialysed against the solution comprising 20 mM Tris–HCl (pH 7.5), 30 mM NaCl, 10 μM $ZnCl_2$ and 5 mM DTT. Finally, Tris was replaced by ^{2}H-labelled Tris using an ultrafiltration cartridge (Millipore). The concentration of wild-type APOBEC3G was 0.1–0.4 mM.

DNA oligomers, synthesized with a DNA synthesizer and purified by reverse-phase HPLC, were purchased (Nippon Seihun).

Gel retardation experiment

^{32}P-labelled DNA (200 nM), d(ATTCCCAATT), was incubated with various concentrations of APOBEC3G (40–80 μM) at 4°C for 1 h in a 10 μl solution comprising 20 mM Tris (pH 7.5), 150 mM NaCl, 10 μM $ZnCl_2$ and 5 mM DTT. The mixtures were run on a 6% polyacrylamide gel containing 45 mM Tris-borate, 150 mM NaCl, 1 mM EDTA, and detected with BAS2000 (Fuji Film).

NMR spectroscopy

NMR spectra were recorded with Bruker DRX800, DRX600 and DRX500 spectrometers equipped with a cryoprobe with a *Z*-gradient. Sequential assignments of the main chain and side chain ^{1}H, ^{13}C and ^{15}N resonances of wild-type APOBEC3G were made in the standard way using triple-resonance NMR spectra (Clore and Gronenborn, 1994), as reported for other proteins (Miyanoiri *et al*, 2003; Enokizono *et al*, 2005). For the chemical shift perturbation experiment, a concentrated DNA solution was added step by step to the APOBEC3G solution up to the APOBEC3G:DNA ratio of 1:10, ^{1}H–^{15}N HSQC spectra being recorded at each step. For real-time monitoring of the cytidine deamination in an NMR tube, a concentrated DNA solution was added at one time to the APOBEC3G solution, the APOBEC3G:DNA ratio being 1:10, and then ^{1}H one-dimensional and ^{1}H–^{13}C HSQC spectra were continuously recorded during the time course of the reaction. The spectra were processed and analysed with XWIN-NMR (Bruker), NMRPipe (Delaglio *et al*, 1995), Sparky (Goddard and Kneller, 2006) and Kujira (Kobayashi *et al*, 2007). Combined chemical shift perturbation as to H^N and N was defined and calculated as $[(\Delta\delta_{HN})^2 + (\Delta\delta_N/5)^2]^{1/2}$ where $\Delta\delta_{HN}$ and $\Delta\delta_N$ are the chemical shift perturbations for H^N and N resonances, respectively. The relative intensity of a ^{1}H–^{15}N correlation peak of the deaminase domain in a free state to that in a complex state was also calculated.

Structure determination

In total, 2380 distance constraints (1117 intra-residue, 581 sequential, 311 medium-range and 371 long-range ones) were obtained from three-dimensional ^{13}C- and ^{15}N-NOESY spectra. In total, 262 backbone dihedral constraints were obtained from TALOS (Cornilescu *et al*, 1999) based on $^{13}C\alpha$, $^{13}C\beta$ and $^{13}C'$ chemical shifts. Additionally, in the later stage of the calculations, 112 distance constraints for 56 hydrogen bonds were included for slowly exchanging amide protons within the identified secondary structure elements. Also, in the later stage, a Zn^{2+} molecule was involved and constrained with respect to the H257, C288 and C291 residues (Prochnow *et al*, 2007; Chen *et al*, 2008) in the structure calculations.

Structure calculations were carried out using distance and dihedral angle constraints (2754 constraints in total) with the simulated annealing protocol supplied with Xplor-NIH v. 2.18 (Schwieters *et al*, 2003). A final set of 10 structures was selected from the 200 calculations on the basis of the criteria of the smallest residual energy values. The quality of the structure was evaluated with PROCHECK (Laskowski *et al*, 1996). Ramachandran plot analysis of the final structures for residues 221–379 showed that 70.6, 25.7, 3.1 and 0.6% were in the most favourable, additionally allowed, generously allowed and disallowed regions, respectively. Coordinates have been deposited in the Protein Data Bank (PDB) with the accession code 2kbo.

Acknowledgements

MK was supported by a Grant-in-Aid for Scientific Research (no. 19036026), PRESTO of JST, and the Strategic Research Project of YCU (no. K20008). TN was supported by a Grant-in-Aid for Scientific Research (no. 2057011) and Strategic Research Project of YCU (no. W20011). This study was supported by a Grant-in-Aid for High Technology Research (HTR) from the Ministry of Education, Science, Sports, and Culture, Japan, research grants from the Human Science Foundation (HIV-K-14719), a Grant-in-Aid for AIDS research from the Ministry of Health, Labour, and Welfare, Japan (H17-AIDS-002), the RIKEN Structural Genomics/Proteomics Initiative (RSGI), the National Project on Protein Structural and Functional Analyses, Ministry of Education, Science, Sports, and Culture, Japan.

References

Beale RC, Petersen-Mahrt SK, Watt IN, Harris RS, Rada C, Neuberger MS (2004) Comparison of the differential context-dependence of DNA deamination by APOBEC enzymes: correlation with mutation spectra *in vivo*. *J Mol Biol* **337:** 585–596

Cen S, Guo F, Niu M, Saadatmand J, Deflassieux J, Kleiman L (2004) The interaction between HIV-1 Gag and APOBEC3G. *J Biol Chem* **279:** 33177–33184

Chelico L, Pham P, Calabrese P, Goodman MF (2006) APOBEC3G DNA deaminase acts processively 3′→5′ on single-stranded DNA. *Nat Struct Mol Biol* **13:** 392–399

Chen KM, Harjes E, Gross PJ, Fahmy A, Lu Y, Shindo K, Harris RS, Matsuo H (2008) Structure of the DNA deaminase domain of the HIV-1 restriction factor APOBEC3G. *Nature* **452:** 116–119

Clore GM, Gronenborn AM (1994) Multidimensional heteronuclear nuclear magnetic resonance of proteins. *Methods Enzymol* **239:** 349–363

Conticello SG, Harris RS, Neuberger MS (2003) The Vif protein of HIV triggers degradation of the human antiretroviral DNA deaminase APOBEC3G. *Curr Biol* **13:** 2009–2013

Cornilescu G, Delaglio F, Bax A (1999) Protein backbone angle restraints from searching a database for chemical shift and sequence homology. *J Biomol NMR* **13:** 289–302

Delaglio F, Grzesiek S, Vuister GW, Zhu G, Pfeifer J, Bax A (1995) NMRPipe: a multidimensional spectral processing system based on UNIX pipes. *J Biomol NMR* **6:** 277–293

Enokizono Y, Konishi Y, Nagata K, Ouhashi K, Uesugi S, Ishikawa F, Katahira M (2005) Structure of hnRNP D complexed with single-stranded telomere DNA and unfolding of the quadruplex by

heterogeneous nuclear ribonucleoprotein D. *J Biol Chem* **280:** 18862–18870

Esnault C, Heidmann O, Delebecque F, Dewannieux M, Ribet D, Hance AJ, Heidmann T, Schwartz O (2005) APOBEC3G cytidine deaminase inhibits retrotransposition of endogenous retroviruses. *Nature* **433:** 430–433

Greene WC (2004) The brightening future of HIV therapeutics. *Nat Immunol* **5:** 867–871

Goddard TD, Kneller DG (2006) *SPARKY 3*. San Francisco: University of California

Harris RS, Bishop KN, Sheehy AM, Craig HM, Petersen-Mahrt SK, Watt IN, Neuberger MS, Malim MH (2003) DNA deamination mediates innate immunity to retroviral infection. *Cell* **113:** 803–809

Harris RS, Liddament MT (2004) Retroviral restriction by APOBEC proteins. *Nat Rev Immunol* **4:** 868–877

Holden LG, Prochnow C, Chang YP, Bransteitter R, Chelico L, Sen U, Stevens RC, Goodman MF, Chen XS (2008) Crystal structure of the anti-viral APOBEC3G catalytic domain and functional implications. *Nature* **456:** 121–124

Kobayashi M, Takaori-Kondo A, Miyauchi Y, Iwai K, Uchiyama T (2005) Ubiquitination of APOBEC3G by an HIV-1 Vif–Cullin5–Elongin B–Elongin C complex is essential for Vif function. *J Biol Chem* **280:** 18573–18578

Kobayashi N, Iwahara J, Koshiba S, Tomizawa T, Tochio N, Guntert P, Kigawa T, Yokoyama S (2007) KUJIRA, a package of integrated modules for systematic and interactive analysis of NMR data directed to high-throughput NMR structure studies. *J Biomol NMR* **39:** 31–52

Laskowski RA, Rullmannn JA, MacArthur MW, Kaptein R, Thornton JM (1996) AQUA and PROCHECK-NMR: programs for checking the quality of protein structures solved by NMR. *J Biomol NMR* **8:** 477–486

Lecossier D, Bouchonnet F, Clavel F, Hance AJ (2003) Hypermutation of HIV-1 DNA in the absence of the Vif protein. *Science* **300:** 1112

Losey HC, Ruthenburg AJ, Verdine GL (2006) Crystal structure of Staphylococcus aureus tRNA adenosine deaminase TadA in complex with RNA. *Nat Struct Mol Biol* **13:** 153–159

Mangeat B, Turelli P, Caron G, Friedli M, Perrin L, Trono D (2003) Broad antiretroviral defence by human APOBEC3G through lethal editing of nascent reverse transcripts. *Nature* **424:** 99–103

Mangeat B, Turelli P, Liao S, Trono D (2004) A single amino acid determinant governs the species-specific sensitivity of APOBEC3G to Vif action. *J Biol Chem* **279:** 14481–14483

Mariani R, Chen D, Schrofelbauer B, Navarro F, Konig R, Bollman B, Munk C, Nymark-McMahon H, Landau NR (2003) Species-specific exclusion of APOBEC3G from HIV-1 virions by Vif. *Cell* **114:** 21–31

Marin M, Rose KM, Kozak SL, Kabat D (2003) HIV-1 Vif protein binds the editing enzyme APOBEC3G and induces its degradation. *Nat Med* **9:** 1398–1403

Marti-Renom MA, Stuar AC, Fiser A, Sanchez R, Melo F, Sali A (2000) Comparative protein structure modeling of genes and genomes. *Annu Rev Biophys Biomol Struct* **29:** 291–325

Mehle A, Strack B, Ancuta P, Zhang C, McPike M, Gabuzda D (2004) Vif overcomes the innate antiviral activity of APOBEC3G by promoting its degradation in the ubiquitin-proteasome pathway. *J Biol Chem* **279:** 7792–7798

Miyanoiri Y, Kobayashi H, Imai T, Watanabe M, Nagata T, Uesugi S, Okano H, Katahira M (2003) Origin of higher affinity to RNA of the N-terminal RNA-binding domain than that of the C-terminal one of a mouse neural protein, musashi1, as revealed by comparison of their structures, modes of interaction, surface electrostatic potentials, and backbone dynamics. *J Biol Chem* **278:** 41309–41315

Muramatsu M, Sankaranand VS, Anant S, Sugai M, Kinoshita K, Davidson NO, Honjo T (1999) Specific expression of activation-induced cytidine deaminase (AID), a novel member of the RNA-editing deaminase family in germinal center B cells. *J Biol Chem* **274:** 18470–18476

Navaratnam N, Morrison JR, Bhattacharya S, Patel D, Funahashi T, Giannoni F, Teng BB, Davidson NO, Scott J (1993) The p27 catalytic subunit of the apolipoprotein B mRNA editing enzyme is a cytidine deaminase. *J Biol Chem* **268:** 20709–20712

Navarro F, Bollman B, Chen H, Konig R, Yu Q, Chiles K, Landau NR (2005) Complementary function of the two catalytic domains of APOBEC3G. *Virology* **333:** 374–386

Prochnow C, Bransteitter R, Klein MG, Goodman MF, Chen XS (2007) The APOBEC-2 crystal structure and functional implications for the deaminase AID. *Nature* **445:** 447–451

Rogozin IB, Iyer LM, Liang L, Glazko GV, Liston VG, Pavlov YI, Aravind L, Pancer Z (2007) Evolution and diversification of lamprey antigen receptors: evidence for involvement of an AID-APOBEC family cytosine deaminase. *Nat Immunol* **8:** 647–656

Schwieters CD, Kuszewski JJ, Tjandra N, Clore GM (2003) The Xplor-NIH NMR molecular structure determination package. *J Magn Reson* **160:** 65–73

Sheehy AM, Gaddis NC, Choi JD, Malim MH (2002) Isolation of a human gene that inhibits HIV-1 infection and is suppressed by the viral Vif protein. *Nature* **418:** 646–650

Shindo K, Takaori-Kondo A, Kobayashi M, Abudu A, Fukunaga K, Uchiyama T (2003) The enzymatic activity of CEM15/Apobec-3G is essential for the regulation of the infectivity of HIV-1 virion but not a sole determinant of its antiviral activity. *J Biol Chem* **278:** 44412–44416

Suspene R, Sommer P, Henry M, Ferris S, Guetard D, Pochet S, Chester A, Navaratnam N, Wain-Hobson S, Vartanian JP (2004) APOBEC3G is a single-stranded DNA cytidine deaminase and functions independently of HIV reverse transcriptase. *Nucleic Acids Res* **32:** 2421–2429

Teh AH, Kimura M, Yamamoto M, Tanaka N, Yamaguchi I, Kumasaka T (2006) The 1.48 A resolution crystal structure of the homotetrameric cytidine deaminase from mouse. *Biochemistry* **45:** 7825–7833

Teng B, Burant CF, Davidson NO (1993) Molecular cloning of an apolipoprotein B messenger RNA editing protein. *Science* **260:** 1816–1819

Wishart DS, Sykes BD (1994) The 13C chemical-shift index: a simple method for the identification of protein secondary structure using 13C chemical-shift data. *J Biomol NMR* **4:** 171–180

Xiang S, Short SA, Wolfenden R, Carter Jr CW (1997) The structure of the cytidine deaminase-product complex provides evidence for efficient proton transfer and ground-state destabilization. *Biochemistry* **36:** 4768–4774

Yu Q, Konig R, Pillai S, Chiles K, Kearney M, Palmer S, Richman D, Coffin JM, Landau NR (2004) Single-strand specificity of APOBEC3G accounts for minus-strand deamination of the HIV genome. *Nat Struct Mol Biol* **11:** 435–442

Yu X, Yu Y, Liu B, Luo K, Kong W, Mao P, Yu XF (2003) Induction of APOBEC3G ubiquitination and degradation by an HIV-1 Vif-Cul5-SCF complex. *Science* **302:** 1056–1060

Zhang H, Yang B, Pomerantz RJ, Zhang C, Arunachalam SC, Gao L (2003) The cytidine deaminase CEM15 induces hypermutation in newly synthesized HIV-1 DNA. *Nature* **424:** 94–98

Virology Journal

BioMed Central

Research

Open Access

Stable replication of the EBNA1/OriP-mediated baculovirus vector and its application to anti-HCV gene therapy

Hitoshi Suzuki[1], Norihiko Matsumoto[1], Tomoyuki Suzuki[1], Myint OO Chang[1] and Hiroshi Takaku*[1,2]

Address: [1]Department of Life and Environmental Sciences, Chiba Institute of Technology, 2-17-1 Tsudanuma, Narashino, Chiba 275-0016, Japan and [2]High Technology Research Center, Chiba Institute of Technology, 2-17-1 Tsudanuma, Narashino, Chiba 275-0016, Japan

Email: Hitoshi Suzuki - g0473021FE@it-chiba.ac.jp; Norihiko Matsumoto - norihiko.matsumoto@it-chiba.ac.jp; Tomoyuki Suzuki - s026079RN@it-chiba.ac.jp; Myint OO Chang - c_myintoo@hotmail.com; Hiroshi Takaku* - hiroshi.takaku@it-chiba.ac.jp

* Corresponding author

Published: 2 October 2009

Virology Journal 2009, **6**:156 doi:10.1186/1743-422X-6-156

Received: 24 June 2009
Accepted: 2 October 2009

This article is available from: http://www.virologyj.com/content/6/1/156

Abstract

Background: Hepatitis C virus (HCV) is one of the main causes of liver-related morbidity and mortality. Although combined interferon-α-ribavirin therapy is effective for about 50% of the patients with HCV, better therapies are needed and preventative vaccines have yet to be developed. Short-hairpin RNAs (shRNAs) inhibit gene expression by RNA interference. The application of transient shRNA expression is limited, however, due to the inability of the shRNA to replicate in mammalian cells and its inefficient transduction. The duration of transgene (shRNA) expression in mammalian cells can be significantly extended using baculovirus-based shRNA-expressing vectors that contain the latent viral protein Epstein-Barr nuclear antigen 1 (EBNA1) and the origin of latent viral DNA replication (OriP) sequences. These recombinant vectors contain compatible promoters and are highly effective for infecting primary hepatocyte and hepatoma cell lines, making them very useful tools for studies of hepatitis B and hepatitis C viruses. Here, we report the use of these baculovirus-based vector-derived shRNAs to inhibit core-protein expression in full-length hepatitis C virus (HCV) replicon cells.

Results: We constructed a long-term transgene shRNA expression vector that contains the EBV *EBNA1* and *OriP* sequences. We also designed baculovirus vector-mediated shRNAs against the highly conserved core-protein region of HCV. HCV core protein expression was inhibited by the EBNA1/OriP baculovirus vector for at least 14 days, which was considerably longer than the 3 days of inhibition produced by the wild-type baculovirus vector.

Conclusion: These findings indicate that we successfully constructed a long-term transgene (shRNA) expression vector (Ac-EP-shRNA452) using the EBNA1/OriP system, which was propagated in *Escherichia coli* and converted into mammalian cells. The potential anti-HCV activity of the long-term transgene (shRNA) expression vector was evaluated with the view of establishing highly effective therapeutic agents that can be further developed for HCV gene therapy applications.

Background

Infection by the hepatitis C virus (HCV) is a major public-health problem, with 170 million people chronically infected worldwide [1,2]. The current treatment with combined interferon-ribavirin therapy fails to cure the infection in 30% to 50% of cases [3,4], particularly those with HCV genotypes 1 and 2. Chronic infection with HCV results in liver cirrhosis and can lead to hepatocellular carcinoma [5,6]. Although combined interferon-α-ribavirin therapy is effective for about 50% of the patients infected with HCV, better therapies are needed and preventative vaccines have yet to be developed. In an effort to develop an alternative to combined interferon-ribavirin treatment, we used RNA interference based on short-hairpin RNA (shRNA), which is a powerful tool for suppressing gene function [7]. Small interference RNAs (siRNAs) directed against HCV are likely to successfully block the replication cycle because HCV is an RNA virus and replicates in the cytoplasm of liver cells without integration into the host genome.

The ability of baculoviruses, including *Autographa californica multiple nuclear polyhedrosis virus* (AcMNPV), to infect insect cells has led to their use in multiple protein expression systems [8,9] and as plant insecticides [10]. AcMNPV, the genome of which comprises a circular, double-stranded DNA that contains ~130 Kbp [11] surrounded by a large envelope, infects a variety of mammalian cell types, with the exception of certain hematopoietic cell lines, although its genome does not replicate or integrate into mammalian chromosomes [12,13]. In particular, the inability of baculoviruses to replicate in mammalian cells makes them attractive candidate vectors for *in vitro* gene therapy studies [14,15]. These recombinant vectors contain compatible promoters and are highly effective in infecting primary hepatocyte and hepatoma cell lines, making them very useful tools for studies of hepatitis B and hepatitis C viruses [16-18].

A major limitation of the baculoviral transduction vector, however, is the short duration of transgene expression. Because the baculovirus genome cannot replicate in mammalian cells, it is usually lost or diluted soon after infection. The efficiency of transgene expression must be substantially increased to be applicable for human gene therapy [19]. The Epstein Barr virus (EBV) plasmid is a replicating episomal vector that has been developed to overcome the problem of rapid elimination of intracellularly-delivered plasmid DNA in nonviral vector-mediated gene transfer. EBV is a gamma herpes virus that is maintained as a ~172-kb episome in a small ratio of resting B cells and epithelial cells in most of the human population. EBV induces latent infection in human B cells [20]. When EBV infects cells, the linear and double-stranded genomes are circularized and sustained as a stable episome. The EBV replication system is present at about 1~100 copies per cell [21], and separates by non-covalent attachment to the host chromosome. The EBV replicon vector system has been used to study long-term transgene expression [22,23]. The origin for latent viral DNA replication (OriP) [24] and the latent viral protein Epstein-Barr nuclear antigen 1 (EBNA1) [21] are essential for the replication of EBV [25]. The *EBNA1/OriP* elements have been successfully exploited to achieve durable expression of foreign genes with plasmid- or virus-based expression systems [26-30].

Previously, we demonstrated efficient inhibition of intracellular HCV replication by baculovirus-based shRNA-expressing vectors [31]. This expression system is transient, however, and therefore unable to provide long-term expression of the shRNA. We hypothesized that long-term transgene (shRNA) expression can be significantly improved in mammalian cells using baculovirus-based shRNA-expressing vectors containing *EBNA1/OriP* sequences.

In the present study, we constructed a long-term transgene (shRNA) expression vector (Ac-EP-shRNA452) using the EBNA1/OriP system, which was propagated in *Escherichia coli* and converted into mammalian cells. The potential anti-HCV activity of the long-term transgene (shRNA) expression vector was evaluated with the view of establishing highly effective therapeutic agents that can be further developed for HCV gene therapy applications.

Results

Construction of baculovirus transfer vectors carrying shRNA-synthesizing cassettes

The core-protein forms the nucleocapsid and modulates gene transcription, cell proliferation, and apoptosis. HCV functions as an mRNA with a single-stranded RNA genome; thus, we hypothesized that cleavage of the core-protein mRNA would inhibit nuclear transport and virus duplication. We previously reported the design of baculovirus vectors expressing shRNA against the following region of the HCV: 452-472, which contains the nuclear localization signal site of the HCV core region (Figure 1A, B) [31]. This vector cannot, however, induce long-term shRNA expression. Therefore, we constructed a long-term transgene shRNA expression vector that contains the EBV *EBNA1* and *OriP* sequences (Figure 1C). Recombinant baculovirus containing the shRNA genome (Ac-shRNA and Ac-EP-shRNA) was generated by homologous recombination of the transfer vector and linearized baculovirus DNAs (BD Biosciences, San Jose, CA) in Sf9 cells. Viruses were produced at high titers, ranging from 2.0×10^8 to 4.5×10^8 pfu/ml.

Inhibition of HCV RNA replication of EBNA1/OriP baculovirus-mediated shRNA-expression vectors in the HCV replicon

We investigated whether the intracellular expression of shRNA inhibited viral replication and affected HCV RNA

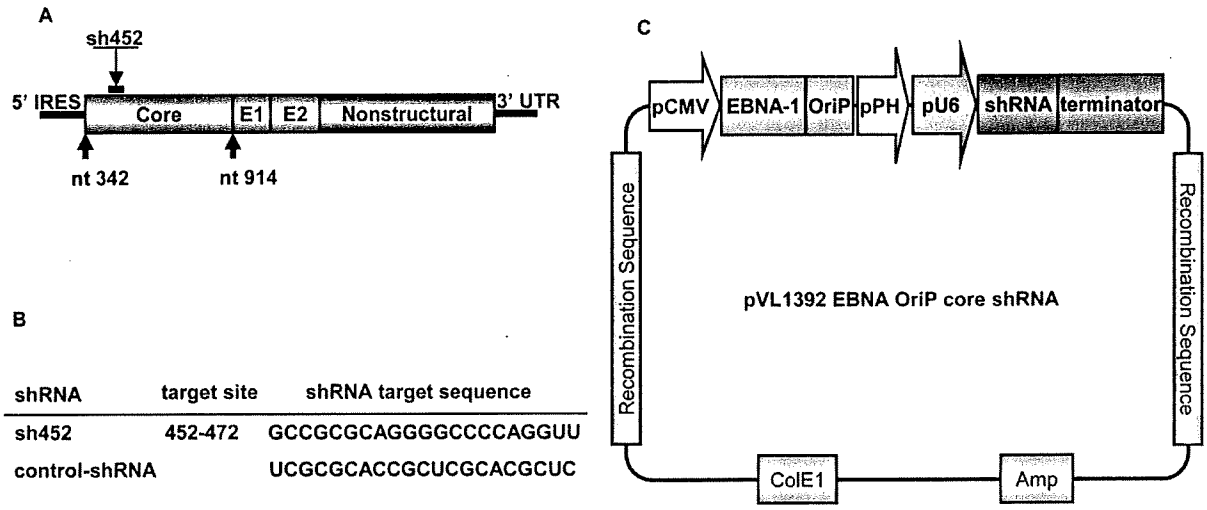

Figure 1
A Genomic profile of HCV showing both coding and non-coding genes. B HCV core region target sites and sequences used for the design of shRNAs. **C** Construction and schematic representation of EBNA1/OriP baculovirus transfer vector expressing HCV core shRNA.

levels in NNC#2 cells. The baculovirus-infection efficiency of NNC#2 cells ranged from 80% to 90% [31]. Real-time reverse transcription polymerase chain reaction (RT-PCR) was used to examine the ability to silence RNA in NNC#2 cells 3 days post-infection. When NNC#2 cells were infected with Ac-shRNAs at a multiplicity of infection (MOI) of 50 and 100, HCV RNA levels were significantly reduced compared with a scrambled shRNA control. Two of the constructs, Ac-shRNA452 (55%, MOI 50; 71%, MOI 100) and Ac-EP-shRNA452 (55%, MOI 50; 67%, MOI 100), inhibited the HCV RNA levels (Figure 2A). In contrast, the control baculovirus vector (Ac-EP-control-shRNA) did not inhibit HCV replication (Figure 2A). These findings indicated that the shRNA had a sequence-specific inhibitory effect on HCV replication. We next used the CLEIA assay to examine whether shRNA against the HCV core protein inhibited viral replication. When NNC#2 cells were infected with Ac-shRNAs at MOIs of 50 and 100, core-protein expression was significantly reduced compared with a non-related shRNA control (Figure 2B). The Ac-EP-control-shRNA baculovirus vectors had no inhibitory effect on HCV replication.

Enhanced baculovirus-mediated shRNA effects were observed in the presence of EBNA1/OriP

To investigate the effect of EBNA/OriP on shRNA expression, we examined the inhibition of HCV replication by Ac-shRNA452 and Ac-EP-shRNA452 in NNC#2 cells for 14 days. When NNC#2 cells were infected with either Ac-shRNA452 or Ac-EP-shRNA452 at an MOI of 100, core-protein expression was significantly reduced compared with a scrambled shRNA control (Ac-EP-control-shRNA) for 3 days (data not shown). Both Ac-shRNA452 and Ac-EP-shRNA inhibited HCV replication for 3 days (Figure 3A). After 3 days, however, cells infected with Ac-shRNA452 exhibited a steady increase in HCV RNA expression while those infected with Ac-EP-shRNA452 continued to have low HCV RNA expression for at least 14 days (Figure 3A). Infection of the NNC#2 cells with recombinant baculovirus vectors containing genetic elements from EBV, EBNA1, and OriP did not induce cellular toxicity, as determined with a bromodeoxyuridine (BrdU)-based colorimetric assay (Figure 3B). These results suggest that HCV RNA expression was more effectively inhibited by the EBNA/OriP baculovirus vector than by the wild-type baculovirus vector.

Production of EBNA1 protein and siRNA by baculovirus-based shRNA-expressing vectors containing EBNA1/OriP sequences

We first used Western blot analysis to detect EBNA1 protein in Ac-EP-shRNA-infected cells (Figure 4A). EBNA1 protein was detected in the Ac-EP-shRNA-infected cells. Then, to investigate whether HCV core gene-targeting shRNAs can be digested to mono-specific products of the expected size, siRNAs were analyzed by Northern blot analysis of shRNA-expressing NNC#2 cells. The siRNAs from both Ac-shRNA452 and Ac-EP-shRNA452 yielded products of ~20 nt, which is the expected size of monomeric siRNAs, for 3 days (Figure 4B). The siRNA band in

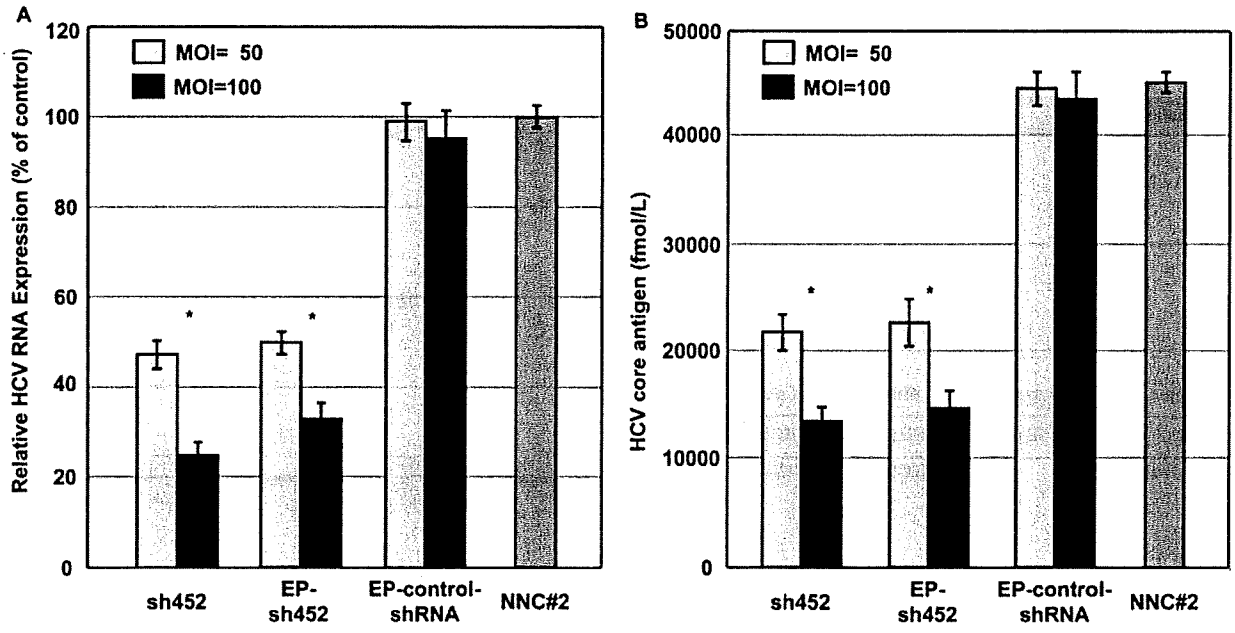

Figure 2
Inhibition of HCV RNA by EBNA1/OriP and wild-type baculovirus-mediated sh452. A Real time PCR analysis of HCV RNA expression after transduction of HCV full replicon cells (NNC#2, 4 × 10^4 cells/well) with an MOI 50 and 100 baculovirus-mediated shRNA. HCV RNA values relative to the scrambled shRNA control are shown. **B** Inhibition of HCV replication by baculovirus-mediated core shRNAs. Ac-shRNAs were used to infect HCV replicons and intracellular HCV core protein levels measured after 3 days by an HCV protein antigen CLEIA assay. Error bars represent standard errors of the mean from three experiments. *$p < 0.01$.

Ac-shRNA452-infected cells, however, became undetectable after 5 days. In contrast, siRNA in Ac-EP-shRNA452-infected cells could be detected for at least 14 days.

Discussion

There is high demand for the development of effective anti-HCV drugs. Gene silencing by RNA interference is a promising approach to elucidate gene function and to inhibit certain RNA viruses such as HCV [32-34]. Delivery of siRNA to the appropriate cells or tissues, however, is a major challenge. Several approaches have been described for generating loss-of function phenotypes in mammalian systems using siRNA, but these techniques are limited and are not suitable for generating a long-term silencing effect *in vivo* [35,36]. Efficient and safe delivery systems have not yet been established for the suppression of HCV replication. Baculoviruses appear to be useful viral vectors, not only for the abundant expression of foreign genes in insect cells, but also for efficient gene delivery to the hepatoma lines HepG2 and Huh7 [37]. One of the major limitations of the baculoviral transduction vector is the short duration of transgene expression. The EBNA1/OriP system has been widely exploited in many different vectors and cell lines. The findings suggest that the EBNA1/OriP system is effective and useful for long-term and high-level transgene expression.

In this study, recombinant baculovirus vectors containing genetic elements from EBV, EBNA1/OriP, which are essential for the episomal maintenance of the EBV genome in latently infected cells, were constructed and tested for their ability to sustain and express the transgene (enhanced HCV core gene-targeting shRNAs) in HCV replicon cells. The introduction of wild-type or EBNA1/OriP-baculovirus-mediated sh452 into target cells containing HCV replicon RNA induced a dose-related reduction in the level of HCV RNA at 3 days. The effectiveness of the inhibition of HCV replication, however, did not differ under the control of the two different vectors (Ac-shRNA452 or Ac-EP-shRNA452).

To investigate the long-term effect of EBNA/OriP on shRNA expression, we examined the inhibition of HCV replication by Ac-shRNA452 and Ac-EP-shRNA452 in NNC#2 cells for 14 days. Both Ac-shRNA452 and Ac-EP-shRNA inhibited HCV replication for 3 days. After 3 days, however, cells infected with Ac-shRNA452 exhibited a steady increase in HCV RNA expression while those

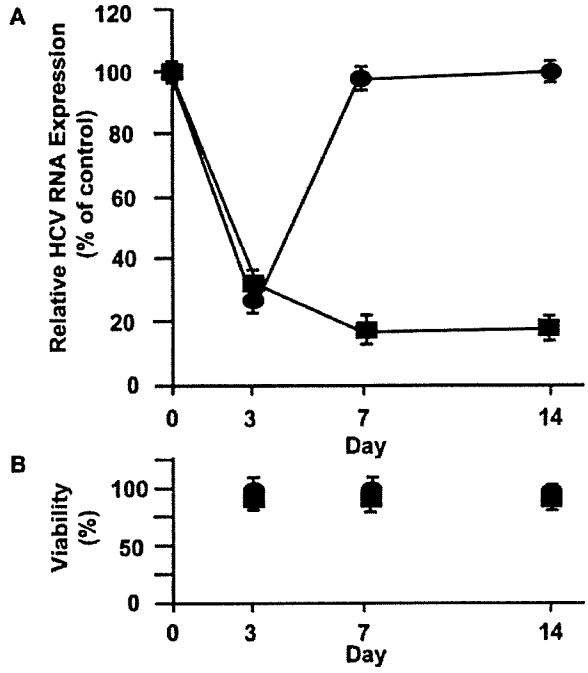

Figure 3
Long-term inhibition of HCV RNA by EBNA1/OriP and wild-type baculovirus-mediated sh452. A Real-time RT-PCR analysis of HCV RNA expression after transduction of HCV full replicon cells (NNC#2, 4 × 10^4 cells/well) with Ac-shRNA452 (MOI = 100 [circle]), Ac-EP-shRNA452 (MOI = 100 [square]). **B** The cytotoxicity of Ac-EP-shRNA452 (square) and Ac-shRNA452 (circle) represented as the percentage reduction of viable Huh-7 cells. A cytotoxicity assay was performed using a BrdU Cell Proliferation ELISA kit according to the manufacturer's instructions (Roche Diagnostics GmbH). The toxicity results are representative of three independent experiments.

infected with Ac-EP-shRNA452 continued to have low HCV RNA expression for at least 14 days. These recombinant baculovirus vectors containing genetic elements from EBV, EBNA1, and OriP did not induce cellular toxicity in the NNC#2 cells, as determined with a BrdU-based colorimetric assay. The HCV RNA was inhibited by EBNA1/OriP baculovirus-mediated shRNA452 for a longer time by the EBNA1/OriP baculovirus vector than by the wild-type baculovirus vector.

To investigate whether EBNA1/OriP baculovirus-mediated shRNA452 can be digested to mono-specific products of expected size, monomeric siRNAs were performed by Northern blot analysis in AB1-shRNA expressing NNC#2 cells. The shRNAs yielded products ~20 nt, the expected size of monomeric siRNAs, over the long term. Furthermore, EBNA1 protein was also detected in the Ac-EP-shRNA-infected cells. These findings indicated a direct correlation between the level of the virus and siRNA or EBNA1 production.

Conclusion

The results of the present study indicate that we have successfully constructed a long-term transgene (shRNA) expression vector (Ac-EP-shRNA452) using the EBNA1/OriP system, which was propagated in *Escherichia coli* and converted into mammalian cells. The potential anti-HCV activity of the long-term transgene (shRNA) expression vector was evaluated with the view of establishing highly effective therapeutic agents that can be further developed for HCV gene therapy applications.

Methods

Cell culture

NNC#2 (NN/1b/FL) cells [38] carrying a full genome replicon were cultured in Dulbecco's modified Eagle's medium supplemented with 10% fetal bovine serum, non-essential amino-acids, L-glutamine, and 1 mg/ml G418 (Invitrogen, Carlsbad, CA).

Northern blot analysis

Total RNA was extracted from Ac-shRNA452 infected Huh7 cells using a mirVana™ miRNA Isolation Kit, according to the manufacturer's instructions (Roche Diagnostics GmbH, Mannheim, Germany). Small RNAs (5 μg) were loaded onto a 15% (w/v) polyacrylamide/7 M urea gel. After transfer to a Hybond-N™ nylon membrane (GE Healthcare Bio-Sciences Corp., Piscataway, NJ), synthetic locked nucleic acid (LNA)/DNA oligonucleotides (sh452: 5'-DIG-CCGCGCAGGGGCCCCAGG-3') complementary to the antisense strand of the shRNA452 were used as probes. The membranes were prehybridized for 1 h in DIG EASY hybridization buffer (Roche Diagnostics GmbH) at 60°C and hybridized overnight to the 5'-DIG labeled LNA/DNA probe (10 ng/ml of hybridization buffer). Four post-hybridization washes were performed for 20 min each at 60°C with 2× SSC (1× SSC = 0.15 M NaCl plus 0.015 M sodium citrate-0.1% sodium dodecyl sulfate). LNA/DNA/RNA hybrids were detected using the CSPD chemiluminescent detection system (Roche Diagnostics GmbH).

Western blot analysis

Cells were lysed in 1× CAT enzyme-linked immunosorbent assay buffer (Roche Diagnostics GmbH). Cell lysates were separated by sodium dodecyl sulfate/polyacrylamide gel electrophoresis and transferred to nitrocellulose membranes, and these were blocked with PVDF Blocking Reagent (TOYOBO, Ohsaka, Japan). The primary antibodies used were monoclonal antibodies against EBNA1 (Acris Antibodies GmbH) and G3PDH (Santa Cruz Biotechnology, Inc., Santa Cruz, CA). Horseradish peroxidase-conju-